Available online at www.sciencedirect.com

ScienceDirect

Geochimica et Cosmochimica Acta 209 (2017) 85–105

Geochimica et Cosmochimica Acta

www.elsevier.com/locate/gca

Iron isotope biogeochemistry of Neoproterozoic marine shales

Marcus Kunzmann [a,b,c,*], Timothy M. Gibson [a], Galen P. Halverson [a], Malcolm S.W. Hodgskiss [a,d], Thi Hao Bui [a], David A. Carozza [a,e], Erik A. Sperling [d], André Poirier [f], Grant M. Cox [a,g], Boswell A. Wing [a,h]

[a] Department of Earth & Planetary Sciences and Geotop, McGill University, Montréal, Québec, Canada
[b] CSIRO Mineral Resources, Australian Resources Research Centre, Kensington, WA 6151, Australia
[c] Northern Territory Geological Survey, Darwin, NT 0800, Australia
[d] Department of Geological Sciences, Stanford University, Stanford, CA, USA
[e] Laboratoire de mathématiques actuarielles et financières, Université du Québec á Montréal, Montréal, Québec, Canada[1]
[f] Département des sciences de la Terre et de l'atmosphère/Geotop, Université du Québec á Montréal, Montréal, Québec, Canada
[g] Department of Earth Sciences, The University of Adelaide, SA 5005, Australia[2]
[h] Department of Geological Sciences, University of Colorado Boulder, UCB 399, Boulder, CO 80309–0399, USA[3]

Received 28 September 2016; accepted in revised form 3 April 2017; Available online 11 April 2017

Abstract

Iron isotopes have been widely applied to investigate the redox evolution of Earth's surface environments. However, it is still unclear whether iron cycling in the water column or during diagenesis represents the major control on the iron isotope composition of sediments and sedimentary rocks. Interpretation of isotopic data in terms of oceanic redox conditions is only possible if water column processes dominate the isotopic composition, whereas redox interpretations are less straightforward if diagenetic iron cycling controls the isotopic composition. In the latter scenario, iron isotope data is more directly related to microbial processes such as dissimilatory iron reduction. Here we present bulk rock iron isotope data from late Proterozoic marine shales from Svalbard, northwestern Canada, and Siberia, to better understand the controls on iron isotope fractionation in late Proterozoic marine environments. Bulk shales span a δ^{56}Fe range from −0.45‰ to +1.04‰. Although δ^{56}Fe values show significant variation within individual stratigraphic units, their mean value is closer to that of bulk crust and hydrothermal iron in samples post-dating the ca. 717–660 Ma Sturtian glaciation compared to older samples. After correcting for the highly reactive iron content in our samples based on iron speciation data, more than 90% of the calculated δ^{56}Fe compositions of highly reactive iron falls in the range from ca. −0.8‰ to +3‰. An isotope mass-balance model indicates that diagenetic iron cycling can only change the isotopic composition of highly reactive iron by <1‰, suggesting that water column processes, namely the degree of oxidation of the ferrous seawater iron reservoir, control the isotopic composition of highly reactive iron. Considering a long-term decrease in the isotopic composition of the iron source to the dissolved seawater Fe(II) reservoir to be unlikely, we offer two possible explanations for the Neoproterozoic δ^{56}Fe trend. First, a decreasing supply of Fe(II) to the ferrous seawater iron reservoir could have caused the reservoir to decrease in size, allowing a higher degree of partial oxidation, irrespective of increasing environmental oxygen levels. Alternatively, increasing oxygen levels would have led to a higher proportion of Fe(II) being oxidized, without decreasing the initial size of the ferrous seawater iron pool. We consider the latter explanation as the most likely. According to this hypothesis, the δ^{56}Fe record reflects the redox evolution of Earth's surface environments. δ^{56}Fe values in pre-Sturtian samples significantly heavier than bulk crust and hydrothermal

* Corresponding author at: CSIRO Mineral Resources, Australian Resources Research Centre, Kensington, WA 6151, Australia.
E-mail address: marcus.kunzmann@csiro.au (M. Kunzmann).
[1] Current address.
[2] Current address.
[3] Current address.

http://dx.doi.org/10.1016/j.gca.2017.04.003

iron imply partial oxidation of a ferrous seawater iron reservoir. In contrast, mean δ^{56}Fe values closer to that of hydrothermal iron in post-Sturtian shales reflects oxidation of a larger proportion of the ferrous seawater iron reservoir, and by inference, higher environmental oxygen levels. Nevertheless, significant iron isotopic variation in post-Sturtian shales suggest redox heterogeneity and possibly a dominantly anoxic deep ocean, consistent with results from recent studies using iron speciation and redox sensitive trace metals. However, the interpretation of generally increasing environmental oxygen levels after the Sturtian glaciation highlights the need to better understand the sensitivity of different redox proxies to incremental changes in oxygen levels to enable us to reconcile results from different paleoredox proxies.

Keywords: Iron isotopes; Neoproterozoic; Diagenesis; Oxygenation; Shale

1. INTRODUCTION

The distribution of iron isotopes in sediments and sedimentary rocks is a powerful measure of the biogeochemical cycle of Fe in the modern and ancient ocean. By far the largest fractionation of Fe isotopes is associated with redox transformation between ferrous and ferric iron (e.g., Schauble et al., 2001; Johnson et al., 2002, 2008b; Welch et al., 2003; Anbar et al., 2005), and hence Fe isotope ratios have been applied to track the evolution of the seawater iron reservoir in response to increasing atmospheric oxygen levels throughout Earth's history (e.g., Rouxel et al., 2005; Planavsky et al., 2012; Fan et al., 2014; Tahata et al., 2015; Zhang et al., 2015). In spite of the dominant role of redox processes in iron isotope fractionation, the interpretation of Fe isotope data from ancient sediments is not straightforward because of different isotopic compositions of iron sources to the ocean and the complex cycling of iron in the water column and during early diagenesis. Nevertheless, distinct features in the iron isotope record appear to broadly correlate with the evolution of atmospheric O_2. The Neoarchean to early Paleoproterozoic (ca. 2.8–2.3 Ga) record comprises highly variable, but typically negative, sedimentary pyrite δ^{56}Fe values (~−3.5‰ to +1.2‰) (Rouxel et al., 2005; Archer and Vance, 2006). Younger Proterozoic (2.3–0.54 Ga) pyrites also span a broad range from ~−2.0‰ to +4.0‰ but are generally less negative (Tahata et al., 2015), whereas Phanerozoic (<0.54 Ga) and modern sedimentary pyrites are also less negative and span a narrower range from ~−1.6‰ to +1.2‰ (e.g., Rouxel et al., 2005; Severmann et al., 2006, 2008; Fehr et al., 2008, 2010). The Fe isotope record of banded iron formation (BIF) and other Fe oxyhydroxide-rich rocks also displays a systematic secular trend. Archean and early Paleoproterozoic iron formation show a large variation in bulk rock δ^{56}Fe values from −2.4‰ to +1.8‰ with most samples displaying heavy isotope ratios (see compilations in Planavsky et al., 2012; Busigny et al., 2014). Younger Fe oxyhydroxide-rich rocks span a narrower range from −0.9‰ to +1.2‰ with most samples falling between −0.5‰ and +0.5‰ (Planavsky et al., 2012; Busigny et al., 2014).

Two broad and contrasting approaches have been implemented in interpreting the record of iron isotopes in the Precambrian. One approach stresses the importance of ferrous iron oxidation across the chemocline in an anoxic Precambrian ocean as the controlling mechanism for the Fe isotopic composition of sedimentary rocks and minerals (Rouxel et al., 2005; Planavsky et al., 2012; Busigny et al., 2014). Whereas quantitative oxidation masks isotope fractionations and produces ferric oxyhydroxides with Fe isotope ratios comparable to the coeval seawater ferrous iron reservoir, non-quantitative oxidation leads to preservation of a significant positive isotope effect upon precipitation of Fe-oxyhydroxides with concomitant depletion of the ferrous iron reservoir (Dauphas et al., 2004; Rouxel et al., 2005; Planavsky et al., 2012; Busigny et al., 2014; Mendes et al., 2017). By extension, lower oxygen concentration in the Neoarchean and early Paleoproterozoic led to incomplete oxidation of the ferrous seawater iron inventory, producing isotopically heavy Fe-oxyhydroxides (precipitated as BIF with heavy δ^{56}Fe) and leaving behind a depleted ferrous reservoir from which pyrites formed (Rouxel et al., 2005; Planavsky et al., 2012). In contrast, higher oxygen levels later in Earth's history allowed for more complete oxidation of ferrous iron, resulting in a narrower range in iron isotope ratios and isotopically heavier pyrites. However, this hypothesis has been challenged because the inferred large negative seawater isotope shift requires that a significant proportion of the dissolved iron inventory precipitated as Fe-oxyhydroxides (50–90%; Yamaguchi and Ohmoto, 2006; Johnson et al., 2008a).

A second approach to interpreting secular trends in the sedimentary iron isotope record emphasizes the importance of diagenetic and microbial processes such that the iron-isotopic composition of BIF and pyrite predominantly reflects dissimilatory iron reduction, which produces large amounts of isotopically light ferrous iron (Johnson et al., 2008a,b; Heimann et al., 2010; Craddock and Dauphas, 2011; Li et al., 2015). In this case, the secular trend in Fe isotopes in the Precambrian is thought to reflect the evolution of heterotrophic organisms, whereas the link to Earth's evolving redox state is ambiguous. This interpretation easily accounts for strongly negative values seen in some samples; however, while diagenetic processes can explain iron isotope partitioning among different mineral phases, shifts in the bulk rock composition require physical separation of distinct iron isotope pools, which is a process that is redox dependent.

A diverse set of redox proxies suggest that atmospheric oxygen levels increased in the Neoproterozoic (e.g., Fike et al., 2006; Canfield et al., 2007; Sahoo et al., 2012; Och and Shields-Zhou, 2012; Ader et al., 2014; Sperling et al., 2015; Kunzmann et al., 2017). However, the degree and

exact timing of oxygenation are not well understood (Sahoo et al., 2012, 2016; Kunzmann et al., 2017; Miller et al., in press). Although iron isotope studies may provide valuable insights, only a small number of iron isotope datasets on the Neoproterozoic have been published (Halverson et al., 2011; Fan et al., 2014; Zhang et al., 2015; Tahata et al., 2015; Cox et al., 2016a). Iron isotope ratios in Sturtian iron formation deposited during post-glacial transgression show a systematic trend of up-section increasing δ^{56}Fe values, which has been interpreted as oxidation of a successively decreasing proportion of the ferrous iron reservoir during deepening of the depositional environment (Halverson et al., 2011; Cox et al., 2016a). Sedimentary pyrites in Cryogenian (ca. 717–635 Ma) black shales from South China show a systematic decrease from positive values (ca. 0‰ to +1‰) to values comparable to hydrothermal iron sources (ca. −0.5‰ to +0‰), which Zhang et al. (2015) interpreted to reflect near-quantitative oxidation of the ferrous iron reservoir and, by inference, increasing environmental oxygen levels. Tahata et al. (2015) reported Fe isotope data from pyrites in carbonates, shales, sandstones, and diamictites from a Neoproterozoic succession in Svalbard and suggested that heavy δ^{56}Fe values before and after the Sturtian glaciation attest to an anoxic-ferruginous deep ocean. The bulk rock Fe isotopic composition of carbonates, phosphorites, and diagenetic chert from the Ediacaran (ca. 635–541 Ma) Doushantuo Formation in South China were also interpreted to reflect a ferruginous deep ocean (Fan et al., 2014). Although these interpretations are broadly consistent with redox constraints from other proxies (e.g., Canfield et al., 2008; Johnston et al., 2010, 2013; Li et al., 2010; Sperling et al., 2013, 2015; Kunzmann et al., 2015), limited data hinders the reconciliation of the iron isotope record with proposed models of oxygenation.

The reconstruction of a detailed secular Fe isotope trend is further complicated because previous studies focused on different rock types and either presented bulk rock or mineral-specific isotope data. Data from specific minerals (like pyrite) yield more pronounced isotopic variations because the biogeochemical signals are undiluted by detrital sedimentary components. However, specific minerals may not fully capture seawater signals. For example, pyrite formed in non-euxinic environments does not quantitatively capture dissolved ferrous iron (Berner, 1984), making it difficult to extract information about changing seawater chemistry. In contrast, although bulk rock analyses include detrital iron sources, this method has the advantage of capturing both diagenetic and water column processes. Furthermore, recrystallization during burial should not affect the bulk rock composition, even though it may redistribute isotopes between individual mineral phases.

Here we report the bulk rock Fe isotope composition of 124 marine shales from Svalbard, northwestern Canada, and Siberia deposited between 1050 and 570 Ma. Our first aim is to evaluate the relative importance of isotopic fractionation in the water column versus fractionation during diagenesis on the bulk shale Fe isotope composition. To address this question, we created an isotope mass-balance model, which suggests that water column processes, i.e. the quantitative or non-quantitative oxidation of a ferrous iron reservoir, are more important than fractionation during diagenesis in setting bulk rock compositions. Based on conclusions drawn from modeling, we qualitatively interpret our new record of the secular variation of Fe isotopes in Neoproterozoic shales (Fig. 1) in the context of the relative proportion of the oxidized Fe(II) pool. Favoring a control by environmental oxygen levels, the Fe isotope record qualitatively suggests an increase in oxygen levels after the 717–660 Ma Sturtian glaciation. Nevertheless, significant iron isotopic variation in post-Sturtian units suggest redox heterogeneity and a deep ocean that possibly remained dominantly anoxic, at least through the mid-Ediacaran.

2. BACKGROUND

2.1. Sources of iron to the ocean

Iron delivered to the modern ocean in suspended or colloidal form by rivers has a δ^{56}Fe composition of −1.0‰ to +0.3‰, but most samples plot in the range of ca. −0.1‰ to +0.3‰ (Beard et al., 2003a; Fantle and DePaolo, 2004; Bergquist and Boyle, 2006; Ingri et al., 2006). However, riverine iron is not a significant source to the open ocean because the ionic strength of seawater neutralizes surface charges of colloidal particles, such that they are efficiently removed in nearshore environments (e.g., Boyle et al., 1974; Boyle and Edmond, 1977; Sholkovitz et al., 1978; Krachler et al., 2010). Therefore, riverine iron transported to the open ocean is effectively restricted to nanoparticulate Fe-oxyhydroxides (Raiswell, 2011b). Additional sources of bioavailable, continent-derived iron to the oceans are icebergs (Raiswell et al., 2008; Raiswell, 2011a) and dust. The latter is an important iron source to the ocean (e.g., Duce and Tindale, 1991; Fung et al., 2000; Jickells et al., 2005) and has an Fe isotopic composition of −0.1‰ to +0.3‰ (Zhu et al., 2000; Beard et al., 2003a,b). Dissolved Fe(II) from continental margin sediments has recently been identified as another important iron source to the water column (Elrod et al., 2004, 2008; Lohan and Bruland, 2008; Cullen et al., 2009; Severmann et al., 2010; John et al., 2012; Conway and John, 2014; Dale et al., 2015), in particular in dust poor regions like the Southern Ocean (Tagliabue et al., 2009). The pore water-derived iron is characterized by light isotopic compositions, ranging from −3.5‰ to −0.5‰ (Severmann et al., 2006, 2010; Bergquist and Boyle, 2006; Staubwasser et al., 2006; Homoky et al., 2009, 2013; Tangalos et al., 2010; Chever et al., 2015). In some exceptions, non-reductive dissolution of Fe-oxyhydroxides can lead to positive δ^{56}Fe values of up to +1.2‰ (Radic et al., 2011; Homoky et al., 2013). Hydrothermal iron ranges from −0.7‰ to −0.1‰ but the mass-weighted average is likely close to the high end (Beard et al., 2003b; Severmann et al., 2004; Johnson et al., 2008b; Klar et al., in press). Although some recent studies indicate that this flux may be more significant than previously thought (Toner et al., 2009; Saito et al., 2013; Conway and John, 2014), the contribution of hydrothermal iron to the modern ocean is generally considered to be small (Lilley et al., 2004). The relative contributions of all Fe

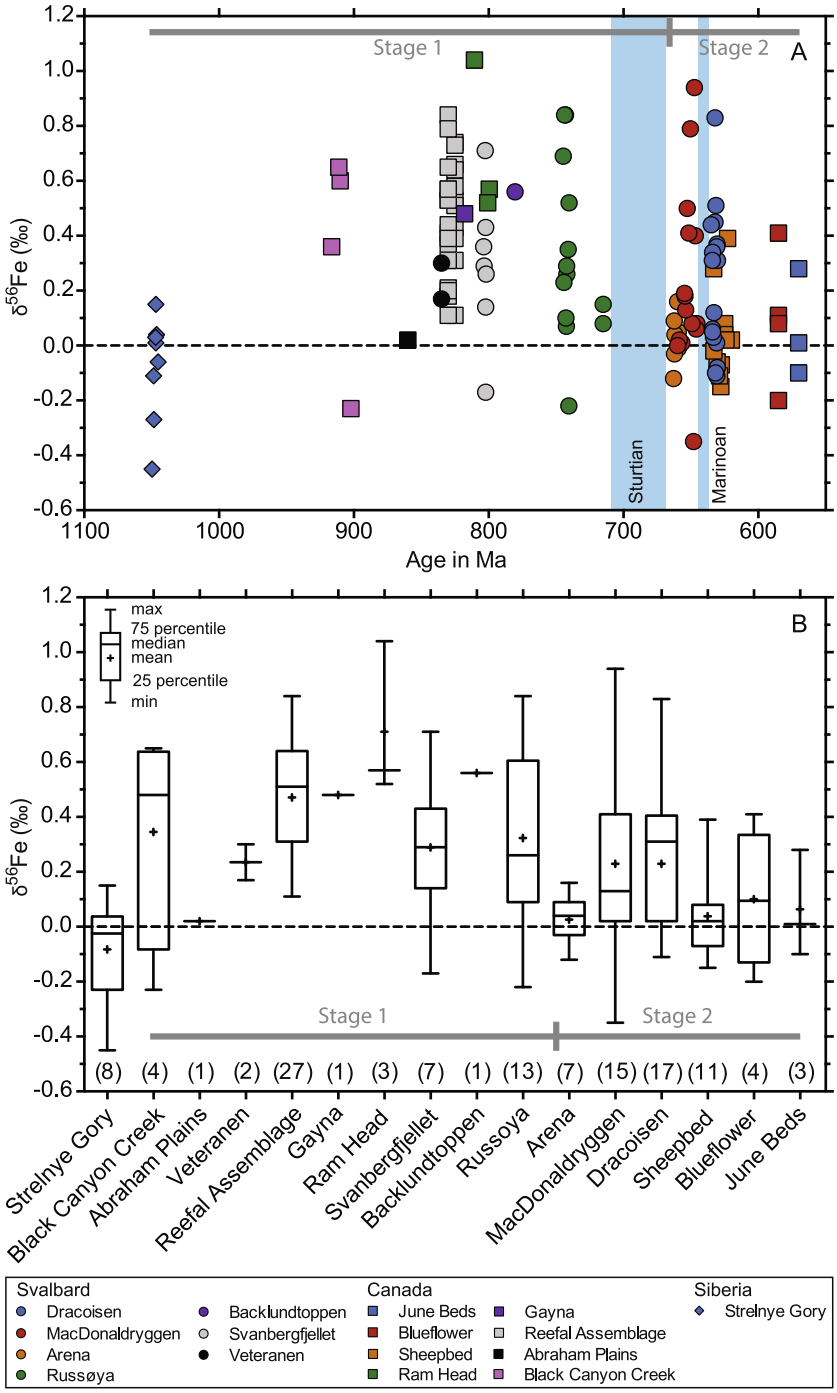

Fig. 1. Bulk shale iron isotope data from late Proterozoic units in Svalbard-East Greenland, northwestern Canada, and Siberia. Analytical error (1SE) is smaller than the symbols. (A) δ^{56}Fe shows significant variation within stratigraphic units. (B) Box plot of δ^{56}Fe for every measured stratigraphic unit. Ediacaran units (Dracoisen, Sheepbed, Blueflower, June Beds) have mean δ^{56}Fe values comparable to the continental crust (ca. +0.09‰). Older units (with the exception of the Strelnye Gory and Arena formations) are dominated by heavier δ^{56}Fe values. The number of samples analyzed for each unit is shown in parentheses. Note that the *x*-axis in (B) is ordered from older (left) to younger (right), but is not exactly plotted in terms of age as shown in (A).

sources to the modern ocean is variable and predominantly depends on geographic location (vicinity to dust, continental margin, and hydrothermal sources) and climate (dry climate promotes dust, glaciated areas decrease the dust flux) (e.g., Conway and John, 2014). Although the same is valid for the Precambrian ocean, hydrothermal iron must have been a much more important iron source due to anoxic and sulfate-poor conditions (e.g., Derry and Jacobsen, 1990; Kump and Seyfried, 2005; Holland, 2006), which allowed the build-up of a significant ferrous seawater reservoir as indicated by the deposition of BIF in the late Archean and early Paleoproterozoic.

2.2. Iron isotope fractionation during diagenesis

Particulate iron delivered to modern marine siliciclastic sediments can be subdivided into an unreactive pool (mainly silicate minerals) and a highly reactive pool, which can undergo reductive dissolution on diagenetic timescales (Canfield, 1989; Raiswell and Canfield, 1998, 2012; Poulton and Canfield, 2011). Reactive iron-bearing minerals include carbonates, Fe-oxyhydroxides, magnetite, and pyrite. Fe-oxyhydroxides are by far the most abundant of these minerals and are mainly formed during pyrite dissolution and oxidation during continental weathering (Reinhard et al., 2013). Common Fe-oxyhydroxides are ferrihydrate, lepicrocite, goethite, and hematite, all of which generally have δ^{56}Fe compositions similar to bulk continental crust (0.09 ± 0.05‰; Beard et al., 2003a). Detrital magnetite and carbonate are proportionately insignificant, and detrital pyrite is limited to the Archean (e.g., Rasmussen and Buick, 1999).

Dissimilatory iron reduction (DIR) is an important pathway of organic matter oxidation in which Fe-oxyhydroxides are used as electron acceptors (e.g., Thamdrup, 2000; Lovley et al., 2004). During DIR, bacteria shuttle electrons to the surface of Fe-oxyhydroxides, either by direct contact with the mineral surface (e.g., *Geobacter sulfureducens*) or by production of chelators that solubilize Fe(III) and release of low molecular weight compounds (e.g., *Shewanella putrefaciens*) that shuttle electrons from the cell to the mineral surface (e.g., Lovley et al., 2004). Furthermore, both types of bacteria can produce pili ('nanowires') for transporting electrons to insoluble Fe-oxyhydroxides (e.g., Gorby et al., 2006). DIR produces aqueous ferrous iron ($Fe(II)_{aq}$) that is isotopically up to ~3‰ lighter ($\Delta^{56}Fe_{Fe(II)-Fe(III)} = -3$‰) than the ferric iron substrate (Beard et al., 1999, 2003a; Icopini et al., 2004; Johnson et al., 2005; Crosby et al., 2005, 2007). The generation of isotopically light $Fe(II)_{aq}$ can be explained by isotope exchange between three iron pools that are formed during DIR (Crosby et al., 2005, 2007): $Fe(II)_{aq}$, Fe(II) that is sorbed onto the surface of the Fe(III)-mineral, and Fe (III) that forms an outer, reactive surface layer of the Fe-oxyhydroxide. The dominant isotope effect is an equilibrium fractionation of ~−3‰ between $Fe(II)_{aq}$ and the reactive Fe(III) layer (Crosby et al., 2005, 2007). The isotopic composition of $Fe(II)_{aq}$ depends on the mass balance between the three reactive iron pools, with a maximum isotopic difference occurring in systems with a small $Fe(II)_{aq}$ pool and most iron residing in the reactive Fe(III) layer (Crosby et al., 2007). With ongoing DIR, both the size and the δ^{56}Fe value of the $Fe(II)_{aq}$ pool increase at the expense of the Fe(III) pool in the surface layer of the mineral (Crosby et al., 2007). The fractionation between the $Fe(II)_{aq}$ and reactive Fe(III) layer is independent of the ferric substrate and the bacterial species, such that the role of bacteria in controlling isotope compositions lies solely in making the Fe(III) of the mineral available for electron and isotopic exchange (Crosby et al., 2007). Indeed, the fractionation of ~−3‰ is equivalent to abiological equilibrium fractionation between hexaquo-$Fe(II)_{aq}$ and hexaquo-$Fe(III)_{aq}$ (Johnson et al., 2002; Welch et al., 2003). Isotopic fractionation during sorption of aqueous $Fe(II)_{aq}$ onto the surface of Fe-oxyhydroxides ($\Delta^{56}Fe_{Fe(II)aq-Fe(II)sorbed}$) is mineral specific and is ~−1.24‰ for goethite (see references therein for older estimates Beard et al., 2010), about −0.8‰ for hydrous ferric oxide (Wu et al., 2011), and about −0.49‰ for hematite (Wu et al., 2009, 2010). In sum, the effect of DIR and/or abiological Fe-oxyhydroxide reduction in natural environments leads to pore waters with isotopically depleted iron.

The isotope effects associated with oxidation of $Fe(II)_{aq}$ to $Fe(III)_{aq}$ (biologically mediated or abiological), subsequent coupled isotope and electron exchange between aqueous Fe(II) and Fe(III) species, followed by precipitation of ferric Fe minerals, have been studied in experiments and natural environments (Bullen et al., 2001; Johnson et al., 2002; Skulan et al., 2002; Welch et al., 2003; Croal et al., 2004; Balci et al., 2006; Jang et al., 2008; Beard et al., 2010; Wu et al., 2011; Frierdich et al., 2014a). The equilibrium fractionation between $Fe(II)_{aq}$ and $Fe(III)_{aq}$ of ca. −3‰ is the dominant isotope effect, likely overwhelming any effect associated with biological oxidation of $Fe(II)_{aq}$ (Balci et al., 2006). These studies have shown the equilibrium fractionation between $Fe(II)_{aq}$ and different Fe-oxyhydroxides to be between −1.24‰ and −1.04‰ for goethite (Beard et al., 2010; Frierdich et al., 2014a), and about −3.2‰ for both hematite (Skulan et al., 2002; Welch et al., 2003; Beard et al., 2010) and hydrous ferric oxide (Wu et al., 2011). A kinetic isotope effect may be imparted during mineral precipitation, but Frierdich et al. (2014b) suggested that, at least in the case of goethite, later isotopic equilibration erases the initial kinetic isotopic signature. Comparable to the reduction of Fe(III) by DIR, oxidation of Fe(II) and subsequent Fe-oxyhydroxide precipitation involves different iron pools; $Fe(II)_{aq}$, Fe(III) of the mineral, Fe(II) sorbed on the mineral surface, and a reactive Fe(III) surface layer (Beard et al., 2010; Wu et al., 2010). Adsorption of Fe(II) on Fe-oxyhydroxide surfaces upon mixing of reduced groundwater with oxic water has been demonstrated to cause significant depletion of heavy isotopes in the aqueous Fe(II) pool (Bullen et al., 2001; Teutsch et al., 2005; Rouxel et al., 2008).

The fate of $Fe(II)_{aq}$ in pore waters that is not oxidized depends on the pore water chemistry and on opportunities for interactions with Fe(III)-oxyhydroxide, dissolved sulfide, or carbonate. In pore waters with low dissolved sulfide and bicarbonate concentrations (and anoxic bottom waters), $Fe(II)_{aq}$ can escape to the water column (Scholz et al., 2014a,b; Dale et al., 2015). However, if the $Fe(II)_{aq}$ ion encounters an Fe(III)-oxydydroxide in anoxic pore waters, magnetite (Fe_3O_4) can form abiologically (e.g., Tamura et al., 1983; Schwertmann, 1988; Lovley, 1990). This reaction is associated with an equilibrium fractionation factor of $\Delta^{56}Fe_{Fe(II)aq-magnetite}$ ~−1.6‰ (Johnson et al., 2005; Frierdich et al., 2014b). Magnetite can also form as a breakdown product of smectite during burial diagenesis (Katz et al., 2000) or can be produced by magnetotactic bacteria (e.g., Blakemore, 1982). However, the amount of magnetite formed by magnetotactic bacteria on a per cell basis is about 5000 times smaller than that indirectly produced by DIR (Frankel, 1987).

Isotope effects between $Fe(II)_{aq}$ and carbonate minerals are poorly studied, but experiments suggest that the fractionation is strongly influenced by the phase and stoichiometry of the carbonate minerals (Johnson et al., 2005). Wiesli et al. (2004) reported an equilibrium fractionation factor for siderite ($\Delta^{56}Fe_{Fe(II)aq-siderite}$) of 0.48‰ based on an abiological experiment. In contrast, Johnson et al. (2005) reported no measurable fractionation for siderite precipitation in biological experiments (including DIR). However, these authors noted a fractionation of 0.9‰ for Ca-substituted siderite and suggested that the substitution of other cations such as Mg and Mn will also result in a significant isotope effect (Johnson et al., 2005).

The isotopic fractionation between aqueous iron species and pyrite under demonstrably equilibrium conditions has not been experimentally determined yet. However, several studies have investigated the fractionation between $Fe(II)_{aq}$ and mackinawite (FeS), a pyrite precursor mineral (Butler et al., 2005; Guilbaud et al., 2010, 2011a,b; Wu et al., 2012). The most recent experiments by Guilbaud et al. (2011b) and Wu et al. (2012) reported an equilibrium fractionation factor of $\Delta^{56}Fe_{Fe(II)aq-FeS} \sim -0.32‰$. The fractionation factor is independent of temperature and pH in low temperature environments; however, mackinawite formed at low pH (<4) may partially record an initial positive kinetic isotope fractionation (Butler et al., 2005; Guilbaud et al., 2010, 2011b). Low pH conditions promote particle coarsening via aggregation, which limits isotopic exchange (Wu et al., 2012). However, this process is unlikely to be important at near-neutral or alkaline pH conditions of diagenetic environments, and Wu et al. (2012) suggest that the initial kinetic fractionation is erased by later isotopic equilibration.

The above discussion focuses on experimentally determined fractionation factors for fluid-mineral pairs, which we have chosen to use in our isotope mass-balance model (see discussion). Although it is difficult to achieve and prove equilibrium in low temperature aqueous systems, the most recent results represent realistic values when compared to the rock record. Nevertheless, we emphasize that significant advances have been made recently in determining equilibrium Fe isotope fractionation factors for aqueous species, fluid-mineral systems, and mineral pairs using first-principles calculations that give reduced partition function ratios, called β-factors (for recent review see Dauphas et al., 2017). Data are available for aqueous Fe species (Anbar et al., 2005; Domagal-Goldman and Kubicki, 2008; Hill and Schauble, 2008), Fe-oxyhydroxides (Polyakov et al., 2007; Blanchard et al., 2009; Dauphas et al., 2012; Blanchard et al., 2015), Fe-sulfides (Blanchard et al., 2009; Polyakov and Soultanov, 2011), and Fe-carbonates (Blanchard et al., 2009; Rustad et al., 2010).

3. GEOLOGICAL SETTING

In the following paragraphs, we briefly summarize the geological setting of the sampled successions. Detailed information on stratigraphic sections, including geographic coordinates, ages, and depositional environments, is provided in the Supplementary Information. The analyzed samples come from three different regions: Svalbard-East Greenland, northwestern Canada, and western Siberia. The sedimentary successions in all three regions are well preserved and are sub-greenschist grade.

The Neoproterozoic succession in Svalbard spans the early and middle Neoproterozoic (ca. 835–630 Ma) and hosts glacial deposits of the ca. 717–660 Ma Sturtian and ca. 635 Ma Marinoan glaciations (e.g., Halverson, 2011; Hoffman et al., 2012). The stratigraphy is almost identical to the Neoproterozoic succession in East Greenland, and it is widely accepted that both were deposited in a single, continuous basin (e.g., Fairchild and Hambrey, 1995; Hoffman et al., 2012). Analyzed samples come from the Veteranen, Akademikerbreen, and Polarisbreen groups. The Veteranen Group is constrained to younger than the ca. 950 Ma basement that occurs below it in Noraustlandet (Gee et al., 1995; Johansson et al., 2000), and it was likely deposited during the initial rift phase of basin development (Maloof et al., 2006). In contrast, the overlying Akademikerbreen and Polarisbreen groups, where almost all of our samples come from, were deposited on a thermally subsiding continental shelf (Maloof et al., 2006). The sampled dark grey to black shales represent the deepest depositional environments recorded in this succession and were deposited at or below storm wave base.

We sampled early and late Neoproterozoic stratigraphic units from northwestern Canada, which are exposed in erosional windows through the Phanerozoic cover. Early Neoproterozoic samples come from the ca. 900–800 Ma Fifteenmile, Hematite Creek, Katherine, and Little Dal groups (e.g., Macdonald et al., 2010, 2012; Macdonald and Roots, 2010; Halverson et al., 2012; Kunzmann et al., 2014). All units were deposited on a stable continental shelf. However, the Reefal Assemblage of the middle Fifteenmile Group was deposited in a basin with complex topography that was inherited from synsedimentary normal faulting during deposition of the lower Fifteenmile Group (Macdonald et al., 2012). Late Neoproterozoic (Ediacaran, i.e. 635–541 Ma) samples come from the Sheepbed, June Beds, and Blueflower formations (Macdonald et al., 2013; Sperling et al., 2016). Although their tectonic setting is not fully understood yet, the Ediacaran units in northwestern Canada likely record the transition from rifting to thermal subsidence and passive margin development (Macdonald et al., 2013). All analyzed samples from northwestern Canada are black shales that were deposited at or below storm wave base.

Our Siberian samples come from the ca. 1050–1040 Ma Strelnye Gory Formation, which belongs to the East Angara terrane of the Yenisey Ridge, a Meso- to Neoproterozoic fold-and-thrust belt (Vernikovsky and Vernikovskaya, 2006; Gallet et al., 2012). The strata are part of a passive margin succession. All samples are black shales that were deposited at or below storm wave base.

4. MATERIALS AND METHODS

4.1. Samples

We measured the bulk rock Fe isotope composition of 124 dark grey to black shales (62 from Svalbard-East

Greenland, 54 from northwestern Canada, 8 from Siberia) ranging in age from ~1050 Ma to 570 Ma (Tab. S1). Fresh outcrops were sampled during mapping and stratigraphic logging over the course of multiple field seasons. We interpret our Fe isotope data in the context of previously reported and new major element (Fe and Al), and iron speciation data (Tab. S1; Kunzmann et al., 2015; Sperling et al., 2016). New elemental and Fe speciation data were obtained using the methods outlined in Kunzmann et al. (2015).

4.2. Sample preparation and Fe isotope measurements

Cleaned and cut samples were powdered in a chrome steel ring mill and combusted at 550°C for 5 h (Dean, 1974). The powdering of soft rock samples like shale leads to negligible addition of iron to samples (Hickson and Juras, 1986; Sperling et al., 2013), minimizing the risk of contamination. Approximately 40 mg powder was digested in a mixture of double-distilled, concentrated HCl-HF-HNO_3, followed by a second digestion step in aqua regia (see Supplementary Information for details). Iron was purified by anion-exchange chromatography in a HCl medium using Bio Rad AG1 X4 resin (200–400 μm mesh) following the steps outlined in Halverson et al. (2011). Iron isotope ratios (δ^{56}Fe and δ^{57}Fe) were measured in a 10 ppm solution on a Nu Plasma II multicollector inductively coupled plasma mass spectrometer (MC-ICP-MS) at the Geotop research center, Montréal. The MC-ICP-MS was operated in high-resolution mode and standard-sample-standard bracketing was used to correct for instrumental mass bias. Measured $^{56}Fe/^{54}Fe$ and $^{57}Fe/^{54}Fe$ ratios are reported relative to IRMM-14 using standard delta notation. We routinely prepared and analyzed the certified reference material BHVO-2 (Hawaiian basalt) and obtained average δ^{56}Fe and δ^{57}Fe values of 0.06 ± 0.03‰ (1SE) and 0.11 ± 0.04‰ (1SE), respectively. These values lie within the range reported in the GeoReM database (Jochum et al., 2005). In addition to BHVO-2, we routinely analyzed an in-house hematite standard and obtained standard errors (1SE) of ±0.03‰ for δ^{56}Fe and ±0.04‰ for δ^{57}Fe.

5. RESULTS

The measured δ^{56}Fe values ($n = 124$) span a range from −0.45‰ to +1.04‰ (Fig. 1A). Although significant isotopic variability is observed in every stratigraphic unit (Fig. 1A), these data show systematic secular variation spanning the Neoproterozoic (Fig. 1B). The mean δ^{56}Fe value increases through the latest Mesoproterozoic to early Neoproterozoic from roughly −0.1‰ in the ca. 1050 Ma Strelnye Gory Formation of Siberia to roughly +0.7‰ in the ca. 800 Ma Ram Head Formation of northwestern Canada. This maximum is followed by a decrease of δ^{56}Fe to values below +0.2‰ (i.e., near crustal values) in units younger than the ca. 717–660 Ma Sturtian glaciation. Samples predating the Sturtian glaciation (stage 1 in Fig. 1) have average δ^{56}Fe values of +0.35‰ (±0.31‰ standard deviation), whereas samples younger than 660 Ma (stage 2 in Fig. 1) have average δ^{56}Fe values of +0.15‰ (±0.26‰ standard deviation). Data in stage 1 is normally distributed (Shapiro–Wilk W-test: $p = 0.87$), whereas values in stage 2 are not ($p = 0.0007$). The two stages are significantly different using both nonparametric Wilcoxon tests and a student's t-test ($p < 0.0001$ in both cases).

The relationships between δ^{56}Fe and total iron/aluminium (FeT/Al), as well as ratios of abundances of various iron pools relative to total iron, are shown in Figs. 2 and 3. Following Poulton and Canfield (2005, 2011), we define highly reactive iron (FeHR) as the sum of iron bound in carbonate minerals (FeCarb), oxyhydroxides (FeOx), mixed valence oxides like magnetite (FeMag), and pyrite (FePy). Total iron is the sum of FeHR and an unreactive iron pool (FeUn), comprising mostly silicate minerals. δ^{56}Fe values generally show a negative relationship with FeT/Al and FeHR/FeT (Fig. 2A, B, D, E, G, H). No clear relationship between FeCarb/FeT and δ^{56}Fe is observed (Fig. 2C, F, I). The Russøya Member of Svalbard (Fig. 3A) and the Sheepbed, Reefal Assemblage, and Black Canyon Creek formations of northwestern Canada (Fig. 3D) show a negative relationship between FeOx/FeT and δ^{56}Fe. No clear relationship is observed for the other stratigraphic units. Furthermore, FeMag/FeT and FePy/FeT ratios do not show clear relationships with δ^{56}Fe values in any unit (Fig. 3B, C, E, F, H, I), with the exception of a minor positive correlation between δ^{56}Fe values and FeMag/FeT in the Strelnye Gory Formation of Siberia (Fig. 3H).

6. DISCUSSION

6.1. Model of the isotopic composition of highly reactive iron

This study is the first attempt towards a bulk rock Fe isotope record for the Neoproterozoic. Therefore, we did not measure individual iron speciation pools to investigate the isotopic composition of highly reactive iron and provide a modeling approach instead. Nevertheless, future analyses of individual iron pools should provide an important test of the modeling approach and the conclusions drawn from it.

6.1.1. Model set-up

To better understand the controls on the Fe isotope composition of Neoproterozoic shales, we developed a steady state isotope mass-balance model that describes the fluxes (ϕ) and isotopic effects (ϵ) associated with the transport and reaction pathways of highly reactive iron in anoxic marine sediments (Fig. 4). The aim of our model is to predict the δ^{56}Fe composition of highly reactive iron ($\delta^{56}Fe_{HR-model}$) and to test the significance of diagenetic processes for the overall Fe isotope composition. These values can be compared to our measured bulk rock δ^{56}Fe after correcting for the unreactive iron content (Fig. 5). The relationship between measured bulk rock δ^{56}Fe and the isotopic composition of highly reactive iron in the same sample can be described as

$$\delta^{56}Fe = FeHR/FeT \times \delta^{56}Fe_{HR-calc} + (1 - FeHR/FeT) \times \delta^{56}Fe_{Un} \quad (1)$$

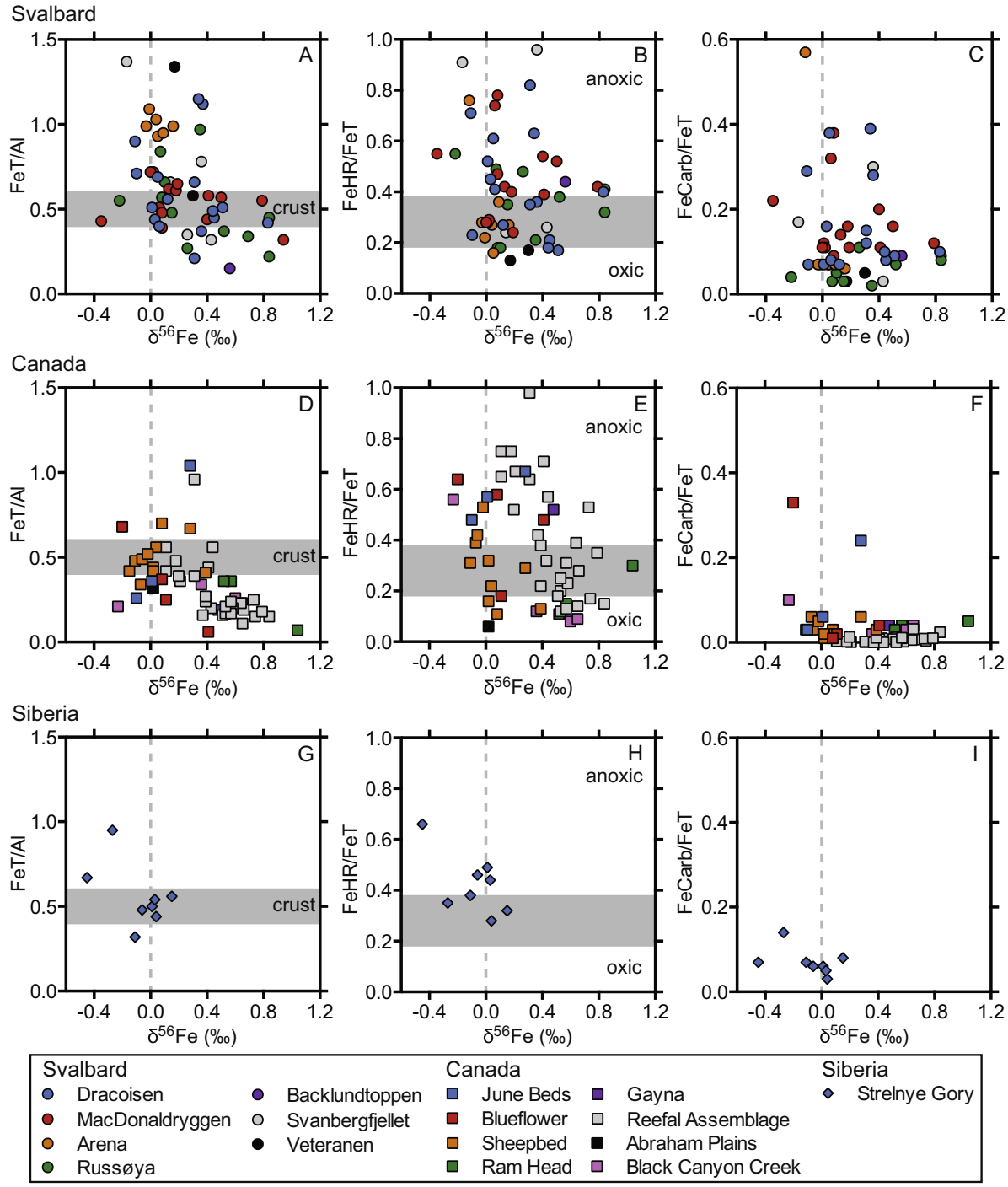

Fig. 2. Relationship between δ^{56}Fe and different iron pools. Analytical error (1SE) is smaller than the symbols. (A) and (B) Negative relationship of FeT/Al and FeHR/FeT with δ^{56}Fe in samples from Svalbard. Grey shaded area in (A) represents typical FeT/Al ratios of the continental crust. Grey shaded field in (B) represents FeHR/FeT ratios that do not distinguish oxic from anoxic conditions (Poulton and Canfield, 2011). (C) The same samples show no clear relationship between δ^{56}Fe and FeCarb/FeT. (D–E) Samples from Canada also show a negative relationship between δ^{56}Fe and FeT/Al and FeHR/FeT, respectively. (F) FeCarb/FeT ratios in shales from Canada are very low and show no systematic relationship with δ^{56}Fe. (G–H) Samples from Siberia also show a negative relationship between δ^{56}Fe and FeT/Al and FeHR/FeT, respectively. (I) No clear relationship between FeCarb/FeT and δ^{56}Fe in shales from Siberia.

where δ^{56}Fe is the measured bulk rock value, $\delta^{56}Fe_{HR-calc}$ is the calculated δ^{56}Fe value for highly reactive iron after correction, and $\delta^{56}Fe_{Un}$ is the isotopic composition of unreactive iron, which we assume to have crustal values (~0.09‰; Beard et al., 2003a). The calculated isotopic composition of highly reactive iron in our samples varies

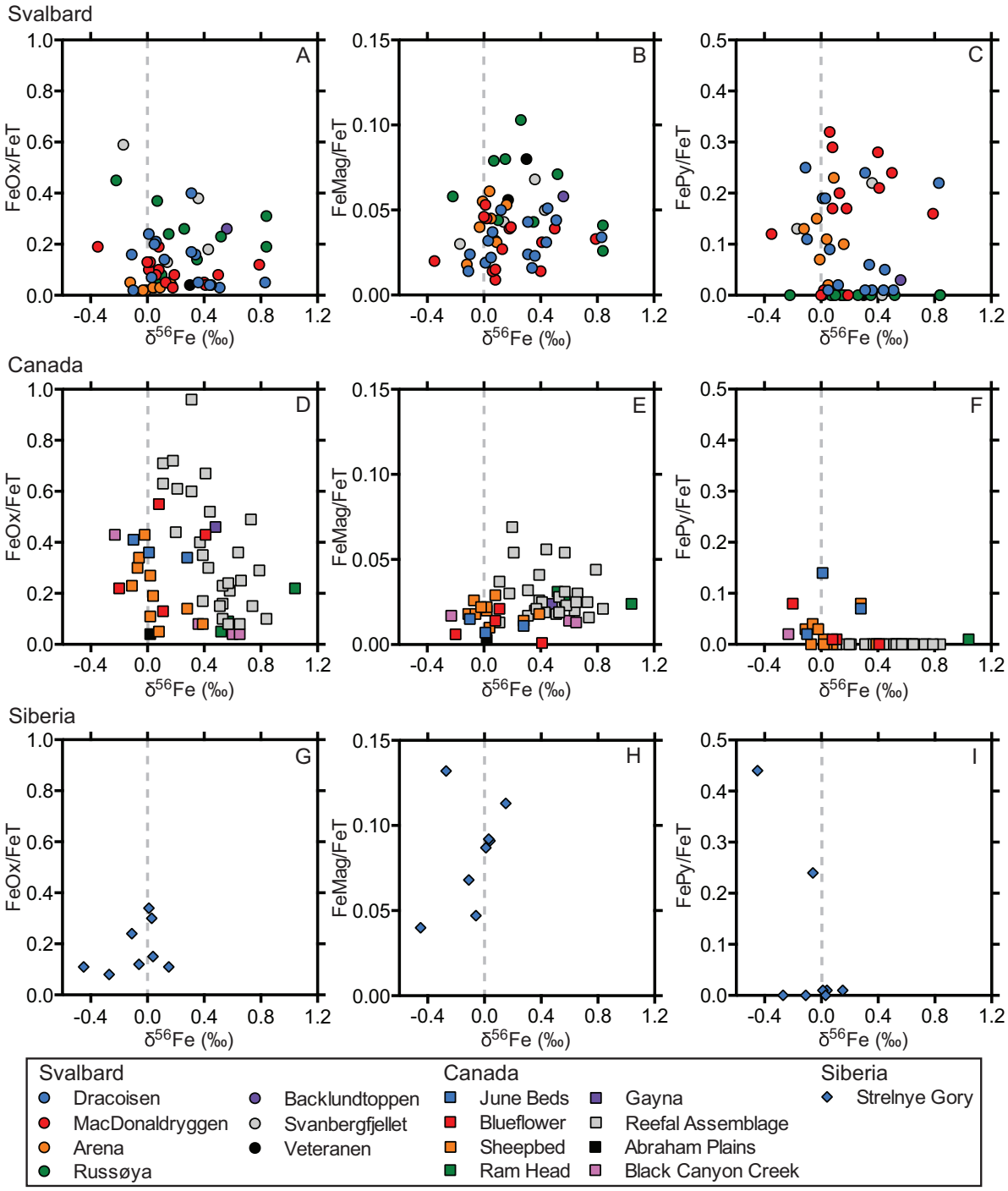

Fig. 3. Relationship between δ^{56}Fe and different iron speciation pools. Analytical error (1SE) is smaller than the symbols. (A–C) The samples from Svalbard show no clear relationship between δ^{56}Fe, FeOx/FeT, FeMag/FeT, and FePy/FeT. One exception is a minor negative relationship between δ^{56}Fe and FeOx/FeT in the Russøya member. (D) Shales from Canada (in particular Reefal Assemblage, Sheepbed, and Black Canyon Creek) show a negative relationship between FeOx/FeT and δ^{56}Fe. (E) and (F) Samples from Canada show no clear relationship between δ^{56}Fe and FeMag/FeT and FePy/FeT, respectively. (G) Siberian samples show no correlation between FeOx/FeT and δ^{56}Fe. (H) Weak positive relationship between δ^{56}Fe and FeMag/FeT in samples from Siberia. (I) The same samples generally have low FePy/FeT ratios with no relationship to δ^{56}Fe.

between ca. −0.8‰ and +7.4‰; however, >90% of our data fall in the range between −0.8‰ and ca. +3‰ (Fig. 5). Samples with extremely high $\delta^{56}Fe_{HR-calc}$ have FeHR/FeT ratios <0.15 and individual Fe pools in these samples generally have a concentration below 0.1 wt.% (Supplementary Information). Although the reproducibility

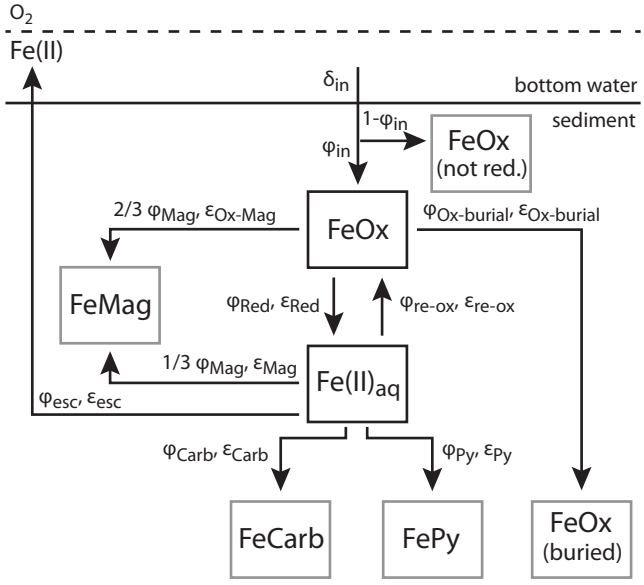

Fig. 4. Schematic diagram of the iron isotope model showing important pathways involved in transport and isotopic fractionation of highly reactive iron in sediments. Each pathway is characterized by a specific flux (ϕ) and isotopic fractionation (ϵ). The fluxes of individual pathways are defined as a proportion of the flux in (ϕ_{in}), which is the reducible fraction of incoming Fe-oxyhydroxides. δ_{in} defines the isotopic composition of incoming oxyhydroxides and is varied in our model to reflect water column processes. Anoxic (ferruginous) bottom waters and sulfide- and bicarbonate-poor pore waters allow escape of some $Fe(II)_{aq}$. Grey boxes represent iron pools that are buried; the $\delta^{56}Fe_{HR-model}$ composition reflects the isotopic composition of individual boxes, considering their respective flux (dictated by the average iron speciation composition). Abbreviations are: Ox-Mag, oxyhydroxide-magnetite; Red, reduction; re-ox, re-oxidation; Ox-burial, oxyhydroxide burial; Mag, magnetite; esc, escape; Carb, carbonate; Py, pyrite.

of sequentially extracted Fe is usually better than ±5% (Kunzmann et al., 2015), the error can significantly increase at the very low concentrations of individual iron pools and very low FeHR/FeT ratios observed in our samples that yield unrealistically high $\delta^{56}Fe_{HR-calc}$ (Sperling et al., 2013, 2015). At concentrations of individual Fe pools below 0.1 wt.%, the error can reach tens of %, and in rare cases, even exceed 100% (see Supplementary Information of Sperling et al., 2013, 2015). However, we emphasize that such high errors do not generally apply to samples with low FeHR/FeT and low concentrations of individual Fe pools. Furthermore, when interpreting paleoredox conditions, a few samples with low FeHR and an associated high error should not influence the basic redox interpretation. For example, doubling the FeHR content (an error of 100%) does not lead to addition of much FeHR when the starting FeHR content is extremely low. However, in our isotopic calculations, errors in the range of tens of % significantly affect $\delta^{56}Fe_{HR-calc}$ (Fig. 5). We conclude that the unrealistically high $\delta^{56}Fe_{HR-calc}$ values can be explained by significant underestimation of the FeHR content, due to very low abundance of FeHR in these samples. With our model, we focus on reproducing the >90% of our data that have $\delta^{56}Fe$ values below +3‰. For these samples, the ratio of the precipitated minerals in our model (Fig. 4; magnetite, carbonate, pyrite, Fe-oxyhydroxides) was set to reflect the average composition of the measured Neoproterozoic shales based on our iron speciation data (Tab. S2).

A description of the model equations is provided in the Supplementary Information; here we emphasize the assumptions and simplifications that are built into the model. First, we assume that the diagenetic cycling of highly reactive iron is fueled by the delivery of Fe-oxyhydroxide phases to the sediment. The Fe-oxyhydroxides settle from the water column and some will also be detrital in origin, escaping near-shore environments. Furthermore, we assume that the detrital flux of carbonate, pyrite, and magnetite is negligible. Consistent with generally low pyrite abundance in our samples, we assume that dissimilatory iron reduction is the major pathway of Fe-oxyhydroxide reduction (e.g., Thamdrup, 2000), rather than reaction with hydrogen sulfide (e.g., Canfield, 1989). Furthermore, we assume that magnetite formed in sediments did not get re-oxidized. The formation of magnetite in our model occurs through the reaction of one $Fe(II)_{aq}$ ion with hydrous ferric oxide (e.g., Lovley, 1990). Other pathways such as the breakdown of smectite during burial (Katz et al., 2000) and formation by magnetotactic bacteria (Blakemore, 1982) are considered negligible and omitted from the model. Other Fe-bearing minerals such as vivianite (a group of ferrous phosphate minerals) are not considered. Moreover, we model all fluxes out of the $Fe(II)_{aq}$ pool to be simultaneous rather than mineral formation in succession.

We varied the isotopic composition of incoming Fe-oxyhydroxides (δ_{in}) between −1‰ and +3‰ (Table 1). The minimum value would reflect oxyhydroxides that precipitate upon quantitative oxidation of hydrothermally derived ferrous iron with a composition of −1‰ (reported values for hydrothermal iron range from −0.7 to −0.1; Sharma et al., 2001; Beard et al., 2003b; Severmann et al., 2004; Klar et al., in press). The maximum value reflects oxi-

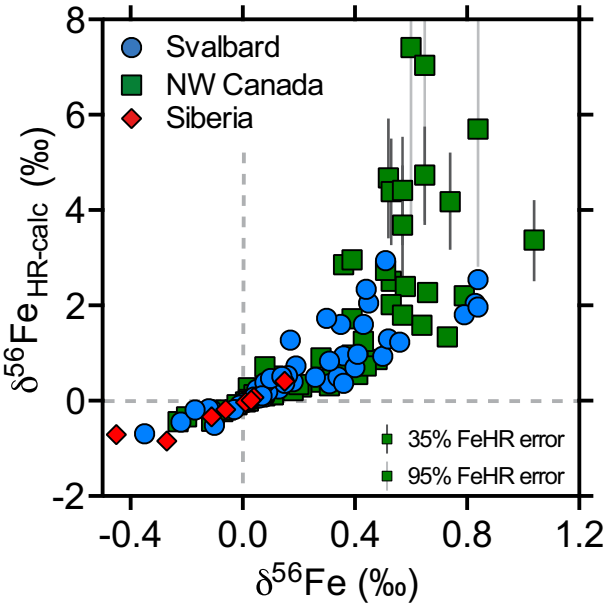

Fig. 5. Bulk rock δ^{56}Fe plotted against the calculated composition of highly reactive iron ($\delta^{56}Fe_{HR-calc}$) following Eq. (1). More than 90% of data have highly reactive iron compositions between −0.8‰ and +3‰. Unrealistically high $\delta^{56}Fe_{HR-calc}$ values can be explained with significant underestimation of FeHR due to very low FeHR contents in these samples (see text for discussion). An error in the determination of FeHR abundance of ca. 35% results in more realistic values for seven of the ten samples. The three samples with extremely high $\delta^{56}Fe_{HR-calc}$ values require an error of >95%.

dation of a minor proportion of the ferrous iron pool with an initial δ^{56}Fe value of 0‰—roughly the high end of reported compositions for hydrothermal iron.

Microbial reduction of Fe-oxyhydroxides (in our model collectively referred to as FeOx; Fig. 4) is limited to amorphous and poorly crystalline compounds, whereas more crystalline minerals like goethite and hematite cannot be efficiently reduced by DIR in natural environments (Lovley and Phillips, 1986a,b; Thamdrup, 2000). Amorphous and poorly crystalline FeOx phases generally make up less than 20% of the total FeOx reservoir in sediments (Thamdrup, 2000), consistent with results from sulfate-poor natural environments that indicate that generally less than 20–30% of the available FeOx is microbially reducible (Lovley and Phillips, 1986a). Furthermore, Fe(II) adsorption onto the surface of FeOx may further hinder efficient reduction of FeOx (Roden, 2004). However, Fe(III) in some clay minerals is also microbially reducible (e.g., Stucki et al., 1987; Kostka et al., 1996; Vorhies and Gaines, 2009) and Fe(III) from clay may represent about 10% of the microbially reducible iron (Wallmann et al., 1993; Thamdrup, 2000). Therefore, we varied the proportion of microbially reducible FeOx in our model runs between 10% and 30%, but also performed runs with 100% to test the most extreme scenario. The significant amount of preserved FeOx remaining in our samples (Tab. S2) is consistent with limited reduction by bacteria. Given that our shales contain organic matter (Kunzmann et al., 2015; Sperling et al., 2016), it is unlikely that FeOx is preserved because reactive organic matter was limiting. It is important to emphasize the observation of non-quantitative reduction of FeOx in natural sediments by dissimilatory iron reducers. Considering isotopic mass balance, this is the most important parameter of the diagenetic iron cycle. If only 10–30% of the deposited FeOx is microbially reducible, mass balance considerations suggest that diagenetic processes should not normally exert a major control on the isotopic composition of highly reactive iron and bulk sediment. Nevertheless, we provide a detailed modeling approach and description to include unknown but potentially important processes like re-oxidation of $Fe(II)_{aq}$ and Fe escape to the water column. As ongoing DIR will produce an $Fe(II)_{aq}$ pool with a δ^{56}Fe composition approaching that of FeOx, the physical separation of $Fe(II)_{aq}$ by escape to the water column may be important and needs to be evaluated.

We varied the Δ^{56}Fe between the initial FeOx and $Fe(II)_{aq}$ between −3‰ and 0‰ to reflect the possible range in fractionation occurring during DIR and to match typical pore water $Fe(II)_{aq}$ compositions (Severmann et al., 2006, 2010; Bergquist and Boyle, 2006; Homoky et al., 2009, 2013; Tangalos et al., 2010). The most recent experimentally determined equilibrium Fe isotope fractionation factors were applied in our model (Table 1; see discussion in chapter 2).

In our model runs presented in Fig. 6, we assume that the flux of iron out of the sediments (ϕ_{esc}) is never less than 50% of the reduced iron produced by DIR and that the relative re-oxidation rate (γ_{re-ox}), i.e., the oxidation of $Fe(II)_{aq}$ back to Fe(III) within sediment pore waters is never less

Table 1
Summary of applied fractionation factors in our model (Fig. 4). References: 1, Johnson et al. (2002), 2, Welch et al. (2003); 3, Crosby et al. (2005), 4, Crosby et al. (2007); 5, Skulan et al. (2002), 6, Wu et al. (2011); 7, Johnson et al. (2005), 8, Frierdich et al. (2014b); 9, Wiesli et al. (2004), 10, Guilbaud et al. (2011b); 11, Wu et al. (2012).

Pathway	Fractionation factor (Δ^{56}Fe)	Reference
FeOx→ $Fe(II)_{aq}$ (ϵ_{Red})	−3‰ to 0‰	1–4
FeOx→ FeMag (ϵ_{Ox-Mag})	0‰	–
FeOx→ FeMag ($\epsilon_{Ox-burial}$)	0‰	–
$Fe(II)_{aq}$→ FeOx (ϵ_{re-ox})	−3‰	5, 6
$Fe(II)_{aq}$→ FeMag (ϵ_{FeMag})	−1.6‰	7, 8
$Fe(II)_{aq}$→ water column (ϵ_{esc})	0‰	–
$Fe(II)_{aq}$→ FeCarb (ϵ_{Carb})	+0.5‰	7, 9
$Fe(II)_{aq}$→ FePy (ϵ_{Py})	−0.32‰	10, 11

than 20%. However, a significant flux of Fe(II) out of sediments simultaneous with re-oxidation of $Fe(II)_{aq}$ to Fe(III) may not be likely for most settings as they generally require different redox conditions. To allow for a benthic Fe flux (i.e. anoxic conditions), the oxidation of $Fe(II)_{aq}$ must occur primarily through anaerobic NO_3^- reduction catalyzed by bacteria (e.g., Konhauser et al., 2011). Although NO_3^- concentrations are generally expected to be low in an anoxic ocean, N isotope data suggest that NO_3^- was probably stable in much of the middle to late Neoproterozoic ocean (Ader et al., 2014), consistent with recent evidence for NO_2^- oxidation at nanomolar oxygen concentrations (Bristow et al., 2016). We stress that the motivation for this modeling exercise is to estimate the highest potential influence of diagenetic iron cycling on the composition of highly reactive iron rather than generate a comprehensive accounting of the Neoproterozoic iron cycle. This approach allows us to consider higher values of γ_{re-ox} and ϕ_{esc}, since lowering them to more realistic ones will only decrease the importance of diagenetic iron cycling on the isotopic composition of highly reactive iron.

6.1.2. Model results

Our model results confirm the expectation that release of dissolved iron from sediments to the water column leaves behind an isotopically enriched (heavy) iron pool (Fig. 6). As emphasized earlier, mass balance considerations suggest that the proportion of microbially reducible FeOx (i.e., amorphous and poorly crystalline phases) exerts a major control on the degree of Fe isotope fractionation during diagenesis. Indeed, our model confirms that the importance of diagenetic iron cycling in setting the overall isotopic composition increases with an increasing proportion of incoming iron that is reducible (ϕ_{in}; Fig. 6A-C). Furthermore, we use our model to test to what degree the physical separation of dissolved $Fe(II)_{aq}$, i.e. release of $Fe(II)_{aq}$ to the water column, increases the δ^{56}Fe composition of the remaining FeHR. Increasing the flux of dissolved iron out

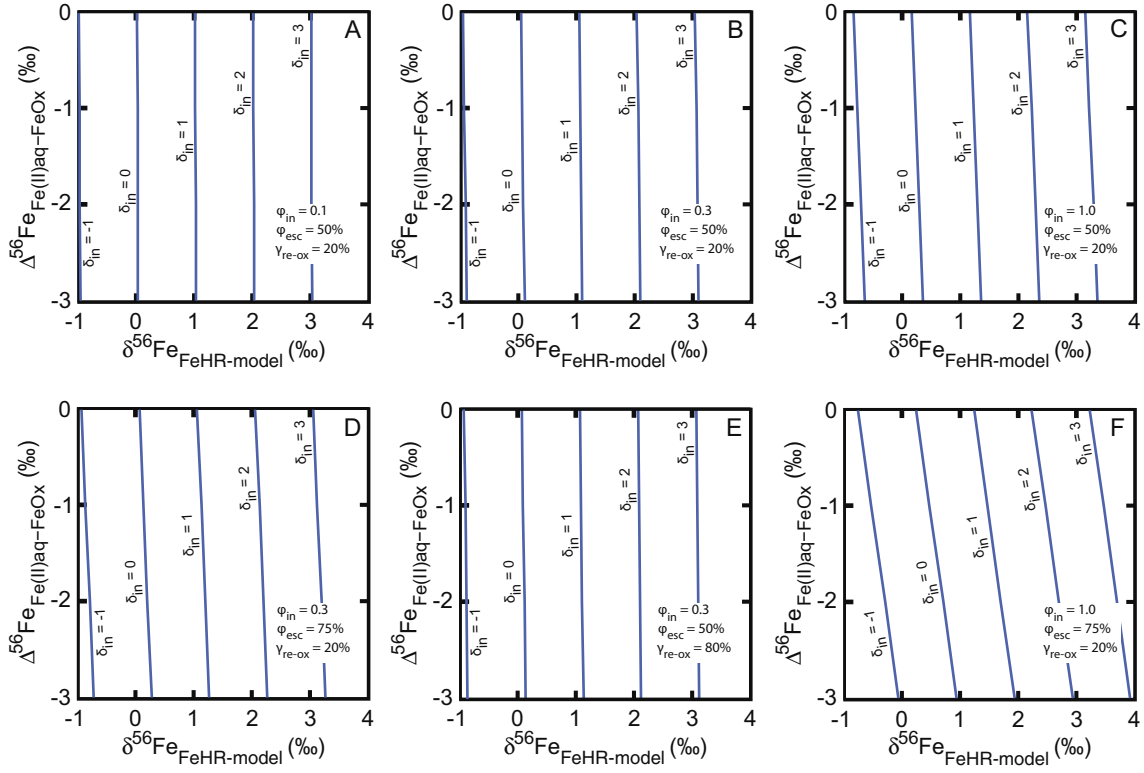

Fig. 6. Results for model runs with different parameter settings. Modeled isotopic composition of highly reactive iron (x-axis) is plotted against different values for isotopic fractionation associated with reduction of FeOx and production of pore water $Fe(II)_{aq}$. The five lines represent different starting compositions of incoming Fe-oxyhydroxides. Mineral compositions are held constant and are set to average iron speciation composition (Supplementary Information; 60% Fe-oxyhydroxides, 20% carbonate, 10% magnetite, 10% pyrite). (A–C) Following mass-balance, increase of ϕ_{in} increases the importance of diagenetic iron cycling and isotope exchange results in residual highly reactive iron with successively heavier δ^{56}Fe values. (D) The residual highly reactive iron becomes progressively heavier with increasing iron flux to the water column (ϕ_{esc}; compare to B). (E) Increasing the re-oxidation rate (γ_{re-ox}) without changing ϕ_{esc} or mineral proportions, does not significantly change isotopic compositions (compare to B). (F) The largest influence of diagenetic iron cycling on the isotopic composition of highly reactive iron occurs when all Fe-oxyhydroxides are reducible and the flux of iron out of sediments is high. Although these parameter settings are unrealistically high for natural environments, this model run demonstrates that diagenetic processes are not as important for the isotopic composition as the starting composition of incoming Fe-oxyhydroxides, i.e. water column processes.

of the sediments from 50% (Fig. 6B) to 75% (Fig. 6D) increases the δ^{56}Fe of highly reactive iron by ca. 0.3‰ (Fig. 6D). Another potentially important process we tested was the influence of the re-oxidation rate of $Fe(II)_{aq}$ to Fe (III) (γ_{re-ox}). An increase of the re-oxidation rate from 20% (Fig. 6B) to 80% only leads to a minor increase in δ^{56}Fe of FeHR when the proportions of formed minerals and their amount (i.e., flux of Fe out of sediments) is held constant (Fig. 6E). Assuming that all of the incoming FeOx is reducible ($\phi_{in} = 1$) and that 75% of the reduced iron is lost to the water column ($\phi_{esc} = 0.75$)—unrealistically high values—the δ^{56}Fe value of highly reactive iron only increases by ~0.9‰ (Fig. 6F).

We conclude from our modeling exercise that diagenetic iron cycling is only of second order importance in setting the isotopic composition of highly reactive iron. Even if all of the incoming Fe-oxyhydroxides are reducible (Fig. 6C, F), diagenetic iron cycling is unable to generate isotopic enrichment in the highly reactive iron pool that is comparable to the Neoproterozoic record. Our $\delta^{56}Fe_{HR-calc}$ values (Fig. 5) can only be reproduced if δ_{in} is varied substantially. As a result, we suggest that the isotopic composition of the incoming Fe-oxyhydroxides is the major control on the δ^{56}Fe composition of highly reactive iron and bulk shale (if FeHR represents most of the total iron). In the following discussion, we focus on interpreting the bulk shale δ^{56}Fe record because in contrast to the δ^{56}Fe composition of FeHR, it also takes into account the FeHR/FeT and FeT/Al ratios, providing further insight into diagenetic and water column iron cycling.

6.2. Iron systematics in Neoproterozoic shales: the effect of iron shuttling

The two potential sources of Fe-oxyhydroxides to sediments in an anoxic ocean are those delivered with the detrital flux, and oxyhydroxides that formed through (partial) oxidation of dissolved ferrous iron in seawater. Fe-oxyhydroxides delivered by modern rivers can be slightly heavier than the continental crust (up to +0.31‰; Ingri et al., 2006) and oxyhydroxides formed in estuaries by partial oxidation of $Fe(II)_{aq}$ in groundwater have been shown to be isotopically heavy, up to +1.5‰ (Rouxel et al., 2008). However, the latter oxyhydroxides stay in the sediment where they formed and are unlikely to be dispersed across the shelf. Similarly, colloidal iron in rivers is mostly trapped in coastal environments and only a small proportion may reach the middle and outer shelf (e.g., Boyle and Edmond, 1977; Poulton and Raiswell, 2002). Furthermore, this proportion likely mostly comprises crystalline FeOx phases (Raiswell, 2011b), which cannot be reduced by dissimilatory iron reducers. Therefore, (partial) oxidation of a ferrous seawater iron reservoir is the most likely source of Fe-oxyhydroxides in our samples (although they need to be deposited relatively quickly to escape reduction in the anoxic water column). As summarized in Section 2.1, besides hydrothermal iron and the likely minor delivery of riverine iron, other potential sources of iron to the ocean include nanoparticulate Fe-oxyhydroxides, icebergs, dust, and iron from continental margins. However, we assume that the ferrous iron reservoir in a dominantly anoxic Proterozoic ocean mainly originated from hydrothermal sources, which have a mass-weighed average of ca. −0.1‰ (Beard et al., 2003b; Severmann et al., 2004; Johnson et al., 2008b; Klar et al., in press). Furthermore, if other sources like dust, icebergs, nanoparticulate or riverine Fe-oxyhydroxides were locally important, their isotopic composition of −0.1‰ to +0.3‰ is comparable to hydrothermal iron, therefore, would not affect our interpretation. The mass of iron potentially sourced by non-reductive dissolution of Fe-oxyhydroxides is unlikely to be significant. Only significant release of dissolved ferrous iron from continental margins may have lowered the isotopic composition of the ferrous seawater iron reservoir. However, it is very unlikely that this contribution would have been extreme enough to produce a ferrous seawater iron inventory with δ^{56}Fe values below −1‰, i.e. outside of the modeled range.

Our model results suggest that the δ^{56}Fe variability in our sample set (e.g., Fig. 2A, D, G) is mostly due to water column processes, i.e. the delivery of Fe-oxyhydroxides from the water column to the sediments. These Fe-oxyhydroxides had a variable δ^{56}Fe composition (δ_{in}) caused by different degrees of partial oxidation of the ferrous seawater iron reservoir, and potentially also by a somewhat varying composition of this reservoir. If this is the only process that influences the δ^{56}Fe composition of our Neoproterozoic sample set, we expect to observe varying enrichments in FeT/Al (controlled by the net enrichment of Fe from the water column) concomitant with variable enrichments in δ^{56}Fe. The Fe isotopic composition would be controlled by the degree of partial oxidation of ferrous iron in seawater, with very heavy isotopic values reflecting a very small proportion of oxidized Fe(II), and less positive values (approaching the source composition), reflecting a larger degree of oxidation. However, we find overall (weak) negative relationships between δ^{56}Fe and FeT/Al, and FeT/Al ratios of some samples are lower than the continental crust (Fig. 2A, D, G), implying that another process also played a role. The observed patterns between δ^{56}Fe and FeT/Al are broadly comparable to patterns in modern marine settings characterized by diagenetic iron cycling and benthic iron shuttling (Severmann et al., 2008; Scholz et al., 2014b). Therefore, we suggest that even though water column iron cycling controlled the isotopic composition of our shales, diagenetic iron cycling contributed to the overall isotopic composition preserved in the geological record.

Studies of two different modern environments have shown evidence for the shuttling of isotopically distinct iron between depositional sites. In euxinic basins like the highly restricted Black Sea, diagenetic reactions such as DIR mobilize reactive and isotopically light iron in suboxic shelf sediments. The iron is transported to the more distal, euxinic basin, where it is quantitatively trapped during syngenetic pyrite formation in the water column, and buried with sediments in the deep basin (Wijsman et al., 2001; Anderson and Raiswell, 2004; Lyons and Severmann, 2006; Severmann et al., 2008). This iron shuttle leads to depleted FeT/Al ratios and high δ^{56}Fe values of shelf sedi-

ments relative to the detrital flux and enriched FeT/Al ratios with negative δ^{56}Fe in euxinic sediments (Severmann et al., 2008). Thus, the iron shuttle in euxinic basins can be identified by a negative relationship between FeT/Al and δ^{56}Fe (Severmann et al., 2008; Fehr et al., 2008; Fehr et al., 2010; Duan et al., 2010; Owens et al., 2012).

In modern, open marine settings, reactive and isotopically light iron is mobilized from sediments where the oxygen minimum zone (OMZ) impinges on the shelf, causing depleted FeT/Al ratios and heavier δ^{56}Fe values than the detrital flux (Scholz et al., 2014b). The mobilized iron is transported laterally in the oxygen-deficient part of the water column and partly precipitated in sediments below the OMZ (Scholz et al., 2014b). This oxidative trapping leads to enriched FeT/Al, but in contrast to euxinic basins, it is associated with heavier δ^{56}Fe values (Scholz et al., 2014b) because Fe-oxyhydroxide formation preferentially consumes the heavy isotope and the reaction is locally non-quantitative. This leads to complex FeT/Al and δ^{56}Fe relationships.

Both modern settings provide a mechanism to generate the observed depleted FeT/Al compositions with respect to the continental crust (Fig. 2A, D, G) by loss of isotopically light iron (formed by DIR) from the sediments to the water column (Severmann et al., 2008; Scholz et al., 2014b). The escape of isotopically light iron to the water column would lead to slight isotopic enrichment in the remaining sedimentary iron inventory, which may have contributed to form some of the isotopically heaviest samples. Importantly, loss of Fe to the water column requires a concentration gradient between pore waters and seawater, as observed for example in the suboxic OMZ off the coast of Peru (Noffke et al., 2012). Hence, even when anoxic deep waters are considered ferruginous as opposed to euxinic, this distinction does not imply high iron concentrations. Indeed, a long-lived, low-Fe ferruginous ocean during the middle and late Proterozoic is consistent with the disappearance of banded iron formation from the geological record 1.8 Ga ago. A negative relationship between δ^{56}Fe and FeHR/FeT (Fig. 2B, E, H) in our sample set confirms that the remobilized iron was part of the highly reactive iron pool. A negative relationship between δ^{56}Fe and FeOx/FeT, at least in some units (Fig. 3D), is consistent with the notion that the shuttled iron was ultimately sourced from Fe-oxyhydroxides that underwent reductive dissolution during diagenesis.

If some of the samples lost Fe during diagenesis, it is also possible that other samples gained iron that was previously lost by sediments at other depositional sites. However, in contrast to clear evidence that Fe must have been lost at some sites (depleted FeT/Al), our data set does not provide unequivocal evidence for the enrichment of such Fe because the vast majority of samples is not characterized by negative δ^{56}Fe values (as would be expected in euxinic basins) and partial precipitation of diagenetically released iron (leading to isotopic enrichments as in OMZ settings) would be masked by a general enrichment of isotopically heavy iron sourced by (partial) oxidation from the ferrous seawater iron reservoir.

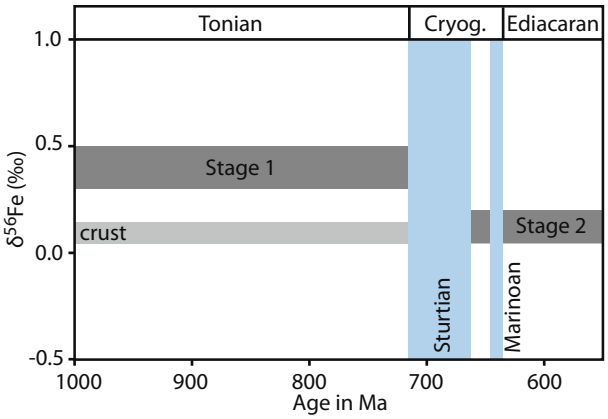

Fig. 7. Simplified evolution of the δ^{56}Fe composition of Neoproterozoic shales (see Fig. 1 for data). Stage 1 is characterized by δ^{56}Fe values mostly ranging from +0.3‰ to +0.5‰. Samples from Stage 2 are mostly in the range from +0.05‰ to +0.2‰, overlapping the composition of the crust. The decrease in δ^{56}Fe indicates more quantitative oxidation of the dissolved Fe(II) reservoir. This can be explained by two different processes: a supply-driven shrinkage of the dissolved ferrous seawater iron reservoir leading to enhanced oxidation without increased environmental oxygen levels, or an increase in oxygen levels leading to enhanced oxidation of the dissolved Fe(II) reservoir without decreasing its initial size. Abbreviation: Cryog., Cryogenian.

An important difference between data from modern samples and our data set is a significantly larger range in δ^{56}Fe values and FeT/Al ratios in Neoproterozoic shales. This expanded range testifies to more intense iron cycling in an anoxic ocean compared to the mostly oxygenated modern ocean.

6.3. The Neoproterozoic iron isotope record: implications for the evolution of Earth's surface environments

Our bulk shale Fe isotope data set (Fig. 1) represents only the first step towards a global Fe isotope record for the Neoproterozoic. A small number of samples (n=<10) were analyzed for most stratigraphic units and the sampled units come from only three regions. Hence the record and our interpretations are provisional and likely need to be revised as new data emerge. Nevertheless, the secular evolution shown by our data set implies a link to the evolution of Neoproterozoic surface environments.

The ca. 1050 Ma Siberian samples from the Strelnye Gory Formation (Fig. 1) on average have negative δ^{56}Fe values, i.e. lighter than the continental crust (+0.09 ± 0.05‰; Beard et al., 2003a). However, the data are too few and too far separated temporally from the remaining data to draw any robust conclusion as to their significance. The remaining data can broadly be divided into two stages (Figs. 1B, 7). Stage 1 comprises all pre-Sturtian units and is characterized by average δ^{56}Fe values of +0.35‰ (±0.31‰ standard deviation; Figs. 1B, 7). This value is heavier than the continental crust (+0.09 ± 0.05‰) and bulk hydrothermal iron (ca. −0.1‰). In contrast, Stage 2 comprises all

post-Sturtian units, which have average δ^{56}Fe values of +0.15‰ (±0.26‰ standard deviation; Figs. 1B, 7). These values overlap with the composition of the continental crust and are slightly higher than the assumed bulk composition of hydrothermal iron (ca. −0.1‰).

We identify three potential mechanisms to explain the observed secular Fe isotope record: a change in the isotopic composition of Fe that sourced the ferrous seawater iron reservoir; supply-dependent shrinkage of the ferrous seawater iron reservoir leading to a higher degree of partial oxidation; or an increase in environmental oxygen levels that led to enhanced partial oxidation.

The isotopic difference between Stages 1 and 2 is ~0.2‰ (Figs. 1, 7), suggesting that the bulk composition of Fe supplied to the ocean (ferrous reservoir) must have also been decreased by ~0.2‰ if this mechanism caused the secular trend. Furthermore, the source must have changed at the time of the Sturtian glaciation and must have kept the new composition for at least the remaining sampled Neoproterozoic to explain our record (Fig. 1). A decrease of the bulk isotopic composition of hydrothermally-derived iron seems unlikely because modern hydrothermal fluids are relatively homogeneous, despite considerable differences in fluid chemistry (e.g., Fe/H_2S ratios) or spreading rates (Severmann et al., 2004). Recently, Cox et al. (2016b) demonstrated a shift in the composition of detrital material across the Sturtian glaciation with continental weathering dominated by mafic material before the glaciation and felsic material in the aftermath of the glaciation. However, this systematic change in weathering regime unlikely influenced the isotopic composition of the ferrous seawater iron reservoir because igneous rocks only show a very small range of δ^{56}Fe compositions (e.g., Beard et al., 2003a; Dauphas et al., 2009; Sossi et al., 2016) and riverine iron is efficiently trapped in near-shore environments (e.g., Boyle et al., 1974; Boyle and Edmond, 1977; Poulton and Raiswell, 2002). Therefore, a higher flux of isotopically light iron from continental shelf sediments to the water column seems to be the only possible process to systematically lower the isotopic composition of dissolved Fe(II) in seawater. This inference implies that more favorable conditions for the release of isotopically light iron from marine sediments emerged following the Sturtian glaciation and were sustained for the remaining sampled Neoproterozoic. This would include increased delivery of amorphous Fe-oxyhydroxides, lower sulfide and bicarbonate concentrations in marine sediments to prevent the formation of iron sulfides and ferrous carbonate minerals, and more widespread anoxic bottom waters to permit realease of Fe(II) to the water column. It is not clear how a systematic change of these requirements could have been sustained from the Sturtian glaciation to at least the late Ediacaran (the younger age limit of our data).

Prolonged contraction of the ferrous seawater iron reservoir following the Sturtian glaciation is another potential explanation for the observed decrease in δ^{56}Fe values because in this scenario, increased environmental oxygen levels are not required to oxidize a larger proportion of the dissolved Fe reservoir. A smaller ferrous seawater iron reservoir may have been facilitated by the deposition of iron formation associated with the Sturtian glaciation (Cox et al., 2013, 2016a), although it is unclear how this nonrecurring process could have permanently decreased the mid- to late Neoproterozoic dissolved Fe(II) reservoir, in particular spanning the following Marinoan global glaciation, without an accompanying decrease in input fluxes to that reservoir. Hence, contraction of the oceanic iron reservoir may potentially be related to less hydrothermal activity. This scenario is intuitively inconsistent with the onset of rifting of the Rodinian super continent about 720 Ma ago (Li et al., 2013), which would be expected to enhance delivery of hydrothermal iron. On the other hand, mantle plume activity, another potentially important source of hydrothermal iron, declined precipitously following emplacement of the ca. 725–710 Ma Franklin LIP (Cox et al., 2016b).

The third potential mechanism to reduce the size of the ferrous iron reservoir is a post-Sturtian rise in atmospheric oxygen, with enhanced oxidation of the ferrous iron reservoir driving the observed decrease in the δ^{56}Fe value of bulk shale. To the degree that the observed decrease in the average bulk shale δ^{56}Fe value of 0.2‰ reflects increasing environmental oxygen levels, our results are consistent with interpretations based on an Fe isotope data set from South China that shows a systematic decrease in pyrite iron-isotopic compositions from 0‰ to +1‰ to values typical for hydrothermal iron (−0.7‰ to −0.1‰), suggesting a Cryogenian increase in oxygen levels (Zhang et al., 2015). Furthermore, a recent compilation of P concentrations in marine sedimentary rocks demonstrates increasing variability and abundance of P in samples deposited after the Sturtian glaciation (Reinhard et al., 2017). This increasing P burial can be explained by decreasing C/P ratios in primary producers, linked to decreasing importance of an Fe-based P trap because bioavailable P is effectively scavenged from an Fe-rich water column through the formation of ferrous phosphate phases and other P-bearing minerals (Reinhard et al., 2017). This interpretation is consistent with our Fe isotope data set, suggesting enhanced oxidation of ferrous iron in post-Sturtian oceans. A recent U isotope data set from Cryogenian non-glacial limestones in Mongolia also indicates post-Sturtian oxygenation (Lau et al., 2017). However, this study highlights that post-Sturtian oxygenation was likely temporarily restricted with a return to more widespread anoxic conditions before the onset of the Marinoan glaciation (Lau et al., 2017). The view of a dominantly anoxic mid-Neoproterozoic ocean is consistent other data sets, namely iron speciation, sulfur isotopes, and redox-sensitive trace element data, which together imply that oxygenation or oxygenation events of the Neoproterozoic ocean were a post-Cryogenian phenomenon (Partin et al., 2013; Kunzmann et al., 2015, 2017; Sperling et al., 2015; Sahoo et al., 2016). The discrepancy between our Fe isotope data set and these studies highlights the need to better understand not only possible short-lived oxygenation events in an otherwise anoxic late Neoproterozoic ocean (Sahoo et al., 2016; Miller et al., in press), but also the fundamental controls on each individual paleoredox proxy and its sensitivity to ambient redox. Such advances will require calibration of proxies in modern environments (e.g., Severmann et al., 2008; Busigny et al., 2014) and will be

informed both by constraints on individual fluid-mineral fractionation factors and results of diagenetic and mass balance modeling. Furthermore, our Fe isotope results only allow qualitative interpretations about first-order changes in oceanic redox conditions and atmospheric oxygen levels. Significant variations in the isotopic composition of individual post-Sturtian shales demonstrate redox heterogeneity and are consistent with recent models of an overall anoxic Ediacaran deep ocean with fluctuating redox conditions (Kendall et al., 2015; Sahoo et al., 2016).

7. CONCLUSION

The data set presented here is the first step towards a bulk shale Fe isotope record for the Neoproterozoic. Isotopic modeling suggests that fractionation associated with the (partial) oxidation of the ferrous seawater iron reservoir is much more important in setting the isotopic composition of shales than diagenetic iron cycling. However, FeT/Al and δ^{56}Fe relationships also demonstrate a second-order contribution of diagenetic iron cycling and benthic iron shuttling. Nevertheless, the dominance of water column iron cycling on the Fe isotopic composition of marine shales permits a qualitative evaluation of the evolution of surface environments in the Neoproterozoic. Our Fe isotope record can be divided into two stages. Stage 1 encompasses samples deposited before the 717–660 Ma Sturtian glaciation and is marked by an average δ^{56}Fe value of +0.35‰ (±0.31‰ standard deviation). In contrast, stage 2 samples postdate the Sturtian glaciation and have an average δ^{56}Fe composition of +0.15‰ (±0.26‰ standard deviation). Potential mechanisms to explain this secular trend include a change in the isotopic composition of iron that sourced the ferrous seawater iron reservoir of the Neoproterozoic ocean; constant environmental oxygen levels but a shrinking ferrous iron reservoir (i.e., decreasing supply), which led to a larger degree of partial oxidation of this reservoir; and increasing environmental oxygen levels that induced a larger degree of partial oxidation of the dissolved Fe(II) pool. Favoring the latter explanation, our data suggest a shift in the mode of iron cycling in the marine realm linked to overall increasing oxygen levels after the 717–660 Ma Sturtian glaciation, although significant variation in the isotopic composition of individual post-Sturtian units suggests redox heterogeneity and a possible dominantly anoxic deep ocean. Whereas the latter conclusion is consistent with recent studies suggesting an overall anoxic Ediacaran deep ocean (Sperling et al., 2015; Kendall et al., 2015; Sahoo et al., 2016), the notion of an overall increase in environmental oxygen levels is an unexpected result. This highlights that reconciling the Fe isotope record with other paleoredox data requires better understanding of the fundamental controls on different redox proxies and their sensitivity to incremental changes in environmental redox conditions. Furthermore, it demonstrates the need to quantify atmospheric oxygen levels, since inconsistent constraints drawn from different proxies might be reconcilable if we better understand what oxygen thresholds lead to non-linear responses in certain proxies.

ACKNOWLEDGMENTS

We thank Silke Severmann, Bjørn Sundby, Peter Crockford, and Al Mucci for informative discussions. Associate Editor Nicolas Dauphas handled the manuscript and also provided excellent comments. We also thank Andrew Heard and an anonymous reviewer for insightful feedback that helped us to improve clarity and the science presented in this paper. This project was supported by the Yukon Geological Survey and grants to Galen Halverson from the Natural Sciences and Engineering Research Council of Canada (NSERC) and the American Chemical Society (Petroleum Research Fund). Boswell Wing acknowledges funding from NSERC and the Fonds de Recherche du Québec-Nature et Technologies (FRQNT). Malcolm Hodgskiss acknowledges support by a NSERC-Undergraduate Student Reserach Award. Marcus Kunzmann acknowledges financial support through scholarships awarded by the Department of Earth & Planetary Sciences, McGill University, and Geotop. Marcus Kunzmann publishes with permission of the Executive Director of the Northern Territory Geological Survey.

APPENDIX A. SUPPLEMENTARY MATERIAL

Supplementary data associated with this article can be found, in the online version, at http://dx.doi.org/10.1016/j.gca.2017.04.003.

REFERENCES

Ader M., Sansjofre P., Halverson G. P., Busigny V., Trindade R. I. F., Kunzmann M. and Nogueira A. C. R. (2014) Ocean redox structure across the late Neoproterozoic oxygenation event: a nitrogen isotope perspective. *Earth Planet. Sci. Lett.* **396**, 1–13.

Anbar A. D., Jarzecki A. A. and Spiro T. G. (2005) Theoretical investigation of iron isotope fractionation between $Fe(H_2O)_6^{3+}$ and $Fe(H_2O)_6^{2+}$: implications for iron stable isotope geochemistry. *Geochim. Cosmochem. Acta* **69**(4), 825–837.

Anderson T. F. and Raiswell R. (2004) Sources and mechanisms for the enrichment of highly reactive iron in euxinic Black Sea sediments. *Am. J. Sci.* **304**, 203–233.

Archer C. and Vance D. (2006) Coupled Fe and S isotope evidence for Archean microbial Fe(III) and sulfate reduction. *Geology* **34** (3), 153–156.

Balci N., Bullen T. D., Witte-Lien K., Shanks W. C., Motelica M. and Mandernack K. W. (2006) Iron isotope fractionation during microbially stimulated Fe(II) oxidation and Fe(III) precipitation. *Geochim. Cosmochem. Acta* **70**, 622–639.

Beard B. L., Handler R. M., Scherer M. M., Wu L., Czaja A. D., Heimann A. and Johnson C. M. (2010) Iron isotope fractionation between aqueous ferrous iron and goethite. *Earth Planet. Sci. Lett.* **295**, 241–250.

Beard B. L., Johnson C. M., Cox L., Sun H., Nealson K. H. and Aguilar C. (1999) Iron isotope biosignatures. *Science* **285**, 1889–1892.

Beard B. L., Johnson C. M., Skulan J. L., Nealson K. H., Cox L. and Sun H. (2003a) Application of Fe isotopes to tracing the geochemical and biological cycling of Fe. *Chem. Geol.* **195**, 87–117.

Beard B. L., Johnson C. M., Von Damm K. L. and Poulson R. L. (2003b) Iron isotope constraints on Fe cycling and mass balance in oxygenated Earth oceans. *Geology* **31**(7), 629–632.

Bergquist B. A. and Boyle E. A. (2006) Iron isotopes in the Amazon River system: weathering and transport signatures. *Earth Planet. Sci. Lett.* **248**, 54–68.

Berner R. A. (1984) Sedimenatry pyrite formation: an update. *Geochim. Cosmochem. Acta* **48**, 605–615.

Blakemore R. P. (1982) Magnetotactic bacteria. *Annu. Rev. Microbiol.* **36**, 217–238.

Blanchard M., Dauphas N., Hu M. Y., Roskosz M., Alp E. E., Golden D. C., Sio C. K., Tissot F. L. H., Zhao J., Gao L., Morris R. V., Fornace M., Floris A., Lazzeri M. and Balan E. (2015) Reduced partition function ratios of iron and oxygen in goethite. *Geochim. Cosmochem. Acta* **151**, 19–33.

Blanchard M., Poitrasson F., Méheut M., Lazerri M., Mauri F. and Balan E. (2009) Iron isotope fractionation between pyrite (FeS_2), hematite (Fe_2O_3) and siderite ($FeCO_3$): a first-principle density functional theory study. *Geochim. Cosmochem. Acta* **73**, 6565–6578.

Boyle E. A., Collier E., T D. A., Edmond J. M., NG A. C. and Stallard R. F. (1974) On the chemical mass-balance in estuaries. *Geochim. Cosmochim. Acta* **38**, 1719–1728.

Boyle E. A. and Edmond J. M. (1977) The mechanism of iron removal in estuaries. *Geochim. Cosmochim. Acta* **41**, 1313–1324.

Bristow L. A., Dalsgaard T., Tiano L., Mills D. B., Bertagnolli A. D., Wright J. J., J H. S., Ulloa O., Canfield D. E., Revsbach N. O. and Thamdrup B. (2016) Ammonium and nitrite oxidation at nanomolar oxygen concentrations in oxygen minimum zone waters. *Proc. Natl. Acad. Sci. USA* **113**(38), 10601–10606.

Bullen T. D., White A. F., Childs C. W., Vivit D. V. and Schulz M. S. (2001) Demonstration of significant abiotic iron isotope fractionation in nature. *Geology* **29**(8), 699–702.

Busigny V., Planavsky N. J., Jezequel D., Crowe S. A., Louvat P., Moureau J., Viollier E. and Lyons T. W. (2014) Iron isotopes in an Archean ocean analogue. *Geochim. Cosmochem. Acta* **133**, 443–462.

Butler I. B., Archer C., Vance D., Oldroyd A. and Rickard D. (2005) Fe isotope fractionation of FeS formation in ambient aqueous solution. *Earth Planet. Sci. Lett.* **236**, 430–442.

Canfield D. E. (1989) Reactive iron in marine sediments. *Geochim. Cosmochim. Acta* **53**, 619–632.

Canfield D. E., Poulton S. W., Knoll A. H., Narbonne G. M., Ross G., Goldberg T. and Strauss H. (2008) Ferruginous conditions dominated later Neoproterozoic deep-water chemistry. *Science* **321**, 949–952.

Canfield D. E., Poulton S. W. and Narbonne G. M. (2007) Late-Neoproterozoic deep-Ocean oxygenation and the rise of animal life. *Science* **315**, 92–95.

Chever F., Rouxel O. J., Croot P. L., Ponzevera E., Wuttig K. and Auro M. (2015) Total dissolvable and dissolved iron isotopes in the water column of the Peru upwelling regime. *Geochim. Cosmochem. Acta* **162**, 66–82.

Conway T. M. and John S. G. (2014) Quantification of dissolved iron sources to the North Atlantic Ocean. *Nature* **511**, 212–215.

Cox G. M., Halverson G. P., Minarik W. G., Le Heron D. P., Macdonald F. A., Bellefroid E. J. and Strauss J. V. (2013) Neoproterozoic iron formation: an evaluation of its temporal, environmental and tectonic significance. *Chem. Geol.* **362**, 232–249.

Cox G. M., Halverson G. P., Poirier A., Le Heron D. P., Strauss J. V. and Stevenson R. S. (2016a) A model for cryogenian iron formation. *Earth Planet. Sci. Lett.* **433**, 280–292.

Cox G. M., Halverson G. P., Stevenson R. S., Vokaty M., Poirier A., Kunzmann M., Li Z.-X., Dudás F. Ö., Strauss J. V. and Macdonald F. A. (2016b) Continental flood basalt weathering as a trigger for Neoproterozoic Snowball Earth. *Earth Planet. Sci. Lett.* **446**, 89–99.

Craddock P. R. and Dauphas N. (2011) Iron and carbon isotope evidence for microbial iron respiration throughout the Archean. *Earth Planet. Sci. Lett.* **303**, 121–132.

Croal L. R., Johnson C. M., Beard B. L. and Newman D. K. (2004) Iron isotope fractionation by Fe(II)-oxidizing photoautotrophic bacteria. *Geochim. Cosmochem. Acta* **68**(6), 1227–1242.

Crosby H. A., Johnson C. M., Roden E. E. and Beard B. L. (2005) Coupled Fe(II)-Fe(III) electron atom exchange as a mechanism for Fe isotope fractionation during dissimilatory iron oxide reduction. *Environ. Sci. Technol.* **39**, 6698–6704.

Crosby H. A., Roden E. E., Johnson C. M. and Beard B. L. (2007) The mechanism of iron isotope fractionation produced during dissimilatory Fe(III) reduction by *Shewanella putrefaciens* and *Geobacter sulfurreducens*. *Geobiology* **5**, 169–189.

Cullen J. T., Chong M. and Ianson D. (2009) British Columbian continental shelf as a source of dissolved iron to the subarctic northeast Pacific Ocean. *Global Biogeochem. Cycles* **23**, GB4012. http://dx.doi.org/10.1029/2008GB003326.

Dale A. W., Nickelsen L., Scholz F., Hensen C., Oschlies A. and Wallmann K. (2015) A revised global estimate of dissolved iron fluxes from marine sediments. *Global Biogeochem. Cycles* **29**, 691–707.

Dauphas N., Craddock P. R., Asimov P. D., Bennett V. C., Nutman A. P. and Ohnenstetter D. (2009) Iron isotopes may reveal the redox conditions of mantle melting from Archean to Present. *Earth Planet. Sci. Lett.* **288**, 255–267.

Dauphas N., John S. G. and Rouxel O. J. (2017) Iron isotope systematics. *Rev. Mineral. Geochem.* **82**, 415–510.

Dauphas N., Roskosz M., Alp E. E., Golden D. C., Sio C. K., Tissot F. L. H., Hu M. Y., Zhao J., Gao L. and Morris R. V. (2012) A *general moment* NRIXS approach to the determination of equilibrium Fe isotopic fractionation factors: application to goethite and jarosite. *Geochim. Cosmochem. Acta* **94**, 254–275.

Dauphas N., van Zuilen M., Madhwa M., Davis A. M., Marty B. and Janney P. E. (2004) Clues from Fe isotope variations on the origin of early Archean BIFs from Greenland. *Science* **306**, 2077–2080.

Dean W. E. (1974) Determination of carbonate and organic matter in calcareous sediments and sedimentary rocks by loss on ignition: comparison with other methods. *J. Sediment. Petrol.* **44**(1), 242–248.

Derry L. A. and Jacobsen S. E. (1990) The chemical evolution of Precambrian seawater: evidence from REEs in banded iron formation. *Geochim. Cosmochem. Acta* **54**, 2965–2977.

Domagal-Goldman S. and Kubicki J. D. (2008) Density functional theory predictions of equilibrium isotope fractionation of iron due to redox changes and organic complexiation. *Geochim. Cosmochem. Acta* **72**, 5201–5216.

Duan Y., Severmann S., Anbar A. D., Lyons T. W., Gordon G. W. and Sageman B. B. (2010) Isotopic evidence for Fe cycling and repartitioning in ancient oxygen-deficient settings: examples from black shales of the mid-to-late Devonian Appalachian basin. *Earth Planet. Sci. Lett.* **290**, 244–253.

Duce R. A. and Tindale N. W. (1991) Chemistry and biology of iron and other trace metals. *Limnol. Oceanogr.* **36**(8), 1715–1726.

Elrod V. A., Berelson W. M., Coale K. H. and Johnson K. S. (2004) The flux of iron from continental shelf sediments: a missing source for global budgets. *Geophys. Res. Lett.* **31**, L12307, p. 1–4.

Elrod V. A., Johnson K. S., Fitzwater S. E. and Plant J. N. (2008) A long-term, high-resolution record of surface water iron concentrations in the upwelling-driven Central California region. *J. Geophys. Res.* **113**, C11021. http://dx.doi.org/10.1029/2007JC004610,2008.

Fairchild I. J. and Hambrey M. J. (1995) Vendian basin evolution in East Greenland and NE Svalbard. *Precambrian Res.* **73**, 217–233.

Fan H., Zhu X., Wen H., Yan B., Li J. and Feng L. (2014) Oxygenation of Ediacaran Ocean recorded by iron isotopes. *Geochim. Cosmochem. Acta* **140**, 80–94.

Fantle M. S. and DePaolo D. J. (2004) Iron isotopic fractionation during continental weathering. *Earth Planet. Sci. Lett.* **228**, 547–562.

Fehr M. A., Andersson P. S., Hålenius U., Gustafsson O. and Mörth C.-M. (2010) Iron enrichments and Fe isotopic compositions of surface sediments from the Gotland Deep, Baltic Sea. *Chem. Geol.* **277**, 310–322.

Fehr M. A., Andersson P. S., Hålenius U. and Mörth C.-M. (2008) Iron isotope variations in Holocene sediments of the Gotland Deep, Baltic Sea. *Geochim. Cosmochem. Acta* **72**, 807–826.

Fike D. A., Grotzinger J. P., Pratt L. M. and Summons R. E. (2006) Oxidation of the Ediacaran Ocean. *Nature* **444**, 744–747.

Frankel R. B. (1987) Anaerobes pumping iron. *Nature* **330**, 208.

Frierdich A. J., Beard B. L., Reddy T. R., Scherer M. M. and Johnson C. M. (2014a) Iron isotope fractionation between aqueous Fe(II) and goethite revisited: new insights based on a multi-direction approach to equilibrium and isotopic exchange rate modification. *Geochim. Cosmochem. Acta* **139**, 383–398.

Frierdich A. J., Beard B. L., Scherer M. M. and Johnson C. M. (2014b) Determination of the $Fe(II)_{aq}$-magnetite equilibrium iron isotope fractionation factor using the three-isotope method and a multi-direction approach to equilibrium. *Earth Planet. Sci. Lett.* **391**, 77–86.

Fung I. Y., Meyn S. K., Tegen I., Doney S. C., John J. G. and Bishop J. K. G. (2000) Iron supply and demand in the upper ocean. *Global Biogeochem. Cycles* **14**(1), 281–295.

Gallet Y., Pavlov V., Halverson G. P. and Hulot G. (2012) Toward constraining trhe long-term reversing behavior of the geodynamo: a new "Maya supercron ~ 1 bilbillion years ago from the magnetostratigraphy of the Kartochka Formation (southwestern Siberia). *Earth Planet. Sci. Lett.*, 117–126.

Gee D. G., Johansson A., Ohta Y., Tebenkov A. M., Krasil'sschikov A. A., Balashov Y. A., Larionov A. N., Gannibal L. F. and Ryungenen G. I. (1995) Grenvillian basement and a major unconformity within the Caledonides of Nordaustlandet, Svalbard. *Precambrian Res.* **70**, 215–234.

Gorby Y. A., Yanina S., McLean J. S., Rosso K. M., Moyles D., Dohnalkova A., Beveridge T. J., Chang I. S., Kim B. H., Kim K. S., Culley D. E., Reed S. B., Romine M. F., Saffarini D. A., Hill E. A., Shi L., Elias D. A., Kennedy D. W., Pinchuk G., Watanabe K., Ishii S., Logan B., Nealson K. H. and Fredrickson J. K. (2006) Electrically conductive bacterial nanowires produced by *Shewanella oneidensis* train MR-1 and other microorganisms. *Proc. Natl. Acad. Sci. (USA)* **103**(30), 11358–11363.

Guilbaud R., Butler I. B. and Ellam R. M. (2011a) Abiotic pyrite formation produces a large Fe isotope fractionation. *Science* **332**, 1548–1551.

Guilbaud R., Butler I. B., Ellam R. M. and Rickard D. (2010) Fe isotope exchange between $Fe(II)_{aq}$ and nanoparticulate mackinawite (FeS_m) during nanoparticle growth. *Earth Planet. Sci. Lett.* **300**, 174–183.

Guilbaud R., Butler I. B., Ellam R. M., Rickard D. and Oldroyd A. (2011b) Experimental determination of the equilibrium Fe isotope fractionation between Fe^{2+}_{aq} and FeS_m (mackinawite) at 25 and 2 °C. *Geochim. Cosmochem. Acta* **75**, 2721–2734.

Halverson G. P. (2011) Glacial sediments and associated strata of the Polarisbreen Group, northeastern Svalbard. In *Geological Record Neoproterozoic Glaciations*, vol. 36, pp. 571–579. Geological Record Neoproterozoic Glaciations. The Geological Society of London, Memoir.

Halverson G. P., Macdonald F. A., Strauss J. V., Smith E. F., Cox G. M. and Hubert-Théou L. (2012) Updated definition and correlation of the lower fifteenmile group in the central and eastern Ogilvie Mountains. In *Yukon Exploration and Geology 2011* (eds. K. MacFarlane and P. Sack). Yukon Geological Survey, pp. 75–90.

Halverson G. P., Poitrasson F., Hoffman P. F., Nédélic A., Montel J.-M. and Kirby J. (2011) Fe isotope and trace element composition of the Neoproterozoic syn-glacial Rapitan iron formation. *Earth Planet. Sci. Lett.* **309**, 100–112.

Heimann A., Johnson C. M., Beard B. L., Valley J. W., Roden E. E., Spicuzza M. J. and Beukes N. J. (2010) Fe, C and O isotope compositions of banded iron formation carbonates demonstrate a major role for dissimilatory iron reduction in ~2.5 Ga marine environments. *Earth Planet. Sci. Lett.* **294**, 8–18.

Hickson C. J. and Juras S. J. (1986) Sample contamination by grinding. *Canadian Mineral.* **24**, 585–589.

Hill P. S. and Schauble E. A. (2008) Modeling the effects of bond environment on equilibrium iron isotope fractionation in ferric aquo-chloro complexes. *Geochim. Cosmochem. Acta* **72**, 1939–1958.

Hoffman P. F., Halverson G. P., Domack E. W., Maloof A. C., Swanson-Hysell N. L. and Cox G. M. (2012) Cryogenian glaciations on the southern tropical paleomargin of Laurentia (NE Svalbard and East Greenland), and a primary origin for the upper Russøya (Islay) carbon isotope excursion. *Precambrian Res.*, 137–158.

Holland H. D. (2006) The oxygenation of the atmosphere and oceans. *Philos. Trans. Roy. Soc. Biol. Sci.* **361**, 903–915.

Homoky W. B., John S. G., Conway T. M. and Mills R. A. (2013) Distinct iron isotopic signatures and supply from marine sediment dissolution. *Nature Commun.* **4**, 2143. http://dx.doi.org/10.1038/ncomms3143.

Homoky W. B., Severmann S., Mills R. A., Statham P. J. and Fones G. R. (2009) Pore-fluid Fe isotopes reflect the extent of benthic Fe redox recycling: evidence from continental shelf and deep sea sediments. *Geology* **37**(8), 751–754.

Icopini G. A., Anbar A. D., Ruebush S. S., Tien M. and Brantley S. L. (2004) Iron isotope fractionation during microbial reduction of iron: the importance of adsorption. *Geology* **32** (3), 205–208.

Ingri J., Malinovsky D., Rodushkin I., Baxter D. C., Widerlund A., Andersson P., Gustafsson O., Forsling W. and Öhlander B. (2006) Iron isotope fractionation in river colloidal matter. *Earth Planet. Sci. Lett.* **245**, 792–798.

Jang J.-H., Mathur R., Liermann L. J., Ruebush S. S. and Brantley S. L. (2008) An iron isotope signature related to electron transfer between aqueous ferrous iron and goethite. *Chem. Geol.* **250**, 40–48.

Jickells T. D., An Z. S., Andersen K. K., Baker A. R., Bergametti G., Brooks N., Cao J. J., Boyd P. W., Duce R. A., Hunter K. A., Kawahata H., Kubiley N., laRoche J., Liss P. S., Mahowald N., Prospero J. M., Ridgwell A. J., Tegen I. and Torres R. (2005) Global iron connections between desert dust, Ocean biogeochemistry, and climate. *Science* **308**, 67–71.

Jochum K. P., Nohl U., Herwig K., Lammel E., Stoll B. and Hofmann A. W. (2005) GeoReM: a new geochemical database for reference materials and isotopic standards. *Geostand. Geoanal. Res.* **29**(3), 333–338.

Johansson A., Larionov A. N., Tebenkov A. M., Gee D. G., Whitehouse M. J. and Vestin J. (2000) Grenvillian magmatism of western and central Nordaustlandet, northeastern Svalbard. *Trans. Roy. Soc. Edinburgh* **90**, 221–234.

John S. G., Mendez J., Moffett J. W. and Adkins J. F. (2012) The flux of iron and iron isotopes from San Pedro Basin sediments. *Geochim. Cosmochem. Acta* **93**, 14–29.

Johnson C. M., Beard B. L., Klein C., Beukes N. J. and Roden E. E. (2008a) Iron isotopes constrain biologic and abiologic processes in banded iron formation genesis. *Geochim. Cosmochem. Acta* **72**, 151–169.

Johnson C. M., Beard B. L. and Roden E. E. (2008b) The iron isotope fingerprints of redox and biogeochemical cycling in Modern and Ancient Earth. *Annu. Rev. Earth Planet. Sci.* **36**, 457–493.

Johnson C. M., Roden E. E., Welch S. A. and Beard B. L. (2005) Experimental constraints on Fe isotope fractionation during magnetite and Fe carbonate formation coupled to dissimilatory hydrous ferric oxide reduction. *Geochim. Cosmochem. Acta* **69** (4), 963–993.

Johnson C. M., Skulan J. L., Beard B. L., Sun H., Nealson K. H. and Braterman P. S. (2002) Isotopic fractionation between Fe (III) and Fe(II) in aqueous solutions. *Earth Planet. Sci. Lett.* **195**, 141–153.

Johnston D. T., Poulton S. W., Dehler C., Porter S., Husson J., Canfield D. E. and Knoll A. H. (2010) An emerging picture of Neoproterozoic ocean chemistry: insights from the Chuar Group, Grand Canyon, USA. *Earth Planet. Sci. Lett.* **290**, 64–73.

Johnston D. T., Poulton S. W., Tosca N. J., O'Brian T., Halverson G. P., Schrag D. P. and Macdonald F. A. (2013) Searching for an oxygenation event in the fossiliferous Ediacaran of northwestern Canada. *Chem. Geol.* **326**, 273–286.

Katz B., Elmore R. D., Cogoini M. and Engel M. H. (2000) Associations between burial diagenesis of smectite, chemical remagnetization, and magnetite authigenesis in the Vocontian trough, SE France. *J. Geophys. Res.* **105**(B1), 851–868.

Kendall B., Komiya T., Lyons T. W., Bates S. M., Gordon G. W., Romaniello S. J., Jiang G., Creaser R. A., Xiao S., McFadden K. A., Sawaki Y., Tahata M., Shu D., Han J., Li Y., Chu X. and Anbar A. D. (2015) Uranium and molybdenum isotope evidence for an episode of widespread ocean oxygenation during the late Ediacaran Period. *Geochim. Cosmochem. Acta* **156**, 173–193.

Klar J. K., James R. H., Gibbs D., Lough A., Parkinson I., Milton J. A., Hawkes J. A. and Conelly D. P. (in press). Isotopic signature of dissolved iron delivered to the Southern Ocean from hydrothermal vents in the East Scotia Sea. *Geology* **45**(4), pp. 351–354. http://dx.doi.org/10.1130/G38432.1.

Konhauser K. O., Kappler A. and Roden E. E. (2011) Iron in microbial metabolisms. *Elements* **7**, 89–93.

Kostka J. E., Stucki J. W., Nealson K. H. and Wu J. (1996) Reduction of structural Fe(III) in smectite by a pure culture of *Shewanella Putrefaciens* strain MR-1. *Clays Clay Miner.* **44**(4), 522–529.

Krachler R., Krachler R. F., von der Kammer F., Süphandag A., Jirsa F., Ayromlou S., Hofmann T. and Keppler B. K. (2010) Relevance of peat-draining rivers for the riverine input of dissolved iron into the ocean. *Sci. Total Environ.* **408**, 2402–2408.

Kump L. R. and Seyfried W. J. (2005) Hydrothermal Fe fluxes during the Precambrian: effect of low oceanic sulfate concentrations and low hydrostatic pressure on the composition of black smokers. *Earth Planet. Sci. Lett.* **235**, 654–662.

Kunzmann M., Bui T. H., Crockford P. W., Halverson G. P., Scott C., Lyons T. W. and Wing B. A. (2017) Bacterial sulfur disproportionation constrains timing of Neoproterozoic oxygenation. *Geology* **45**(3), 207–210.

Kunzmann M., Halverson G. P., Macdonald F. A., Hodgskiss M., Sansjofre P. D., Schumann D. and Rainbird R. H. (2014) The early Neoproterozoic Chandindu formation of the fifteenmile group in the Ogilvie Mountains. In *Yukon Exploration and Geology 2013* (eds. K. E. MacFarlane, M. G. Nordling and P. J. Sack). Yukon Geological Survey, pp. 93–107.

Kunzmann M., Halverson G. P., Scott C. T., Minarik W. G. and Wing B. A. (2015) Geochemistry of Neoproterozoic black shales from Svalbard: implications for oceanic redox conditions spanning Cryogenian glaciations. *Chem. Geol.* **417**, 383–393.

Lau K. V., Macdonald F. A., Maher K. and Payne J. L. (2017) Uranium isotope evidence for temporary ocean oxygenation in the aftermath of the Sturtian Snowball Earth. *Earth Planet. Sci. Lett.* **458**, 282–292.

Li C., Love G. D., Lyons T. W., Fike D. A., Sessions A. L. and Chu X. (2010) A stratified redox model for the Ediacaran ocean. *Science* **328**, 80–83.

Li W., Beard B. L. and Johnson C. M. (2015) Biologically recycled continental iron is a major component in banded iron formations. *Proc. Natl. Acad. Sci. USA* **112**(27), 8193–8198.

Li Z.-X., Evans D. A. D. and Halverson G. P. (2013) Neoproterozoic glaciations in a revised global paleogeography from the break-up of Rodinia to the assembly of Gondwanaland. *Sediment. Geol.* **294**, 219–232.

Lilley M. D., Feely R. A. and Trefry J. H. (2004) Chemical and biochemical transformations in hydrothermal plumes. In *Seafloor Hydrothermal Systems: Physical, Chemcial, Biological, and Geological Interactions*, vol. 91 (eds. S. Humphris, R. A. Zierenberg, L. Mullineaux and R. Thomson). American Geophysical Union Monograph, pp. 369–391.

Lohan M. C. and Bruland K. W. (2008) Elevated Fe(II) and dissolved Fe in hypoxic shelf waters off Oregon and Washington: an enhanced source of iron to coastal upwelling regimes. *Environ. Sci. Technol.* **42**(17), 6462–6468.

Lovley D. R. (1990) Magnetite formation during microbial dissimilatory iron reduction. In *Iron Biominerals* (eds. R. B. Frankel and R. P. Blakemore). Plenum Press, New York, pp. 151–166.

Lovley D. R., Holmes D. E. and Nevin K. P. (2004) Dissimilatory Fe(III) and Mn(IV) Reduction. *Adv. Microb. Physiol.* **49**, 219–286.

Lovley D. R. and Phillips E. J. P. (1986a) Availability of ferric iron for microbial reduction in bottom sediments of the freshwater tidal potomac river. *Appl. Environ. Microbiol.* **52**(4), 751–757.

Lovley D. R. and Phillips E. J. P. (1986b) Organic matter mineralization with reduction of ferric iron in anaerobic sediments. *Appl. Environ. Microbiol.* **51**(4), 683–689.

Lyons T. W. and Severmann S. (2006) A critical look at iron paleoredox proxies: new insights from modern euxinic marine basins. *Geochim. Cosmochim. Acta* **70**, 5698–5722.

Macdonald F. A., Halverson G. P., Strauss J. V., Smith E. F., Cox G. M., Sperling E. A. and Roots C. F. (2012) Early Neoproterozoic basin formation in Yukon, Canada: implications for the make-up and break-up of Rodinia. *Geosci. Canada* **39**, 77–99.

Macdonald F. A. and Roots C. F. (2010) Upper fifteenmile group in the Ogilvie Mountains and correlations of early Neoproterozoic strata in the northern Cordillera. In *Yukon Exploration and Geology 2009* (eds. K. E. MacFarlane, L. H. Weston and L. R. Blackburn). Yukon Geological Survey, pp. 237–252.

Macdonald F. A., Schmitz M. D., Crowley J. L., Roots C. F., Jones D. S., Maloof A. C., Strauss J. V., Cohen P. A., Johnston T. D. and Schrag D. P. (2010) Calibrating the cryogeniation. *Science* **327**, 1241–1243.

Macdonald F. A., Strauss J. V., Sperling E. A., Halverson G. P., Narbonne G. M., Johnston D. T., Kunzmann M., Schrag D. P. and Higgins J. A. (2013) The stratigraphic relationship between the Shuram carbon isotope excursion, the oxygenation of

Neoproterozoic oceans, and the first appearance of the Ediacara biota and bilaterian trace fossils in northwestern Canada. *Chem. Geol.* **362**, 250–272.

Maloof A. C., Halverson G. P., Kirschvink J. L., Schrag D. P., Weiss B. P. and Hoffman P. F. (2006) Combined paleomagnetic, isotopic, and stratigraphic evidence for true polar wander from the Neoproterozoic Akademikerbreen Group, Svalbard, Norway. *Geol. Soc. Am. Bull.* **118**(9/10), 1099–1124.

Mendes M., Lobato L., Kunzmann M., Halverson G. P. and Rosière C. A. (2017) Iron isotope and REE+Y composition of Paleoproterozoic banded iron formation and related iron ores in the Quadrilátero Ferrìfero, Brazil. *Mineral. Deposita* **52**, 159–180.

Miller A. J., Strauss J. V., Halverson G. P., Macdonald F. A., Johnston D. T. and Sperling E. A. (in press) Tracking the onset of phanerozoic-style redox-sensitive trace metal enrichments: new results from basal Ediacaran post-glacial strata in NW Canada. *Chem. Geol.* **457**, pp.24–37. http://dx.doi.org/10.1016/j.chemgeo.2017.03.010.

Noffke A., Hensen C., Sommer S., Scholz F., Bohlen L., Mosch T., Graco M. and Wallmann K. (2012) Benthic iron and phosphorous fluxes across the Peruvian oxygen minimum zone. *Limnol. Oceanogr.* **57**(3), 851–867.

Och L. M. and Shields-Zhou G. A. (2012) The Neoproterozoic oxygenation event: enviornmental pertubations and biogeochemcial cycling. *Earth-Sci. Rev.* **110**, 26–57.

Owens J. D., Lyons T. W., Li X., Macleod K. G., Gordon G., Kuypers M. M. M., Anbar A. D., Kuhnt W. and Severmann S. (2012) Iron isotope and trace metal records of iron cycling in the proto-North Atlantic during the Cenomanian-Turonian oceanic anoxic event (OAE-2). *Paleoceanography* **27**(3), PA3223.

Partin C. A., Bekker A., Planavsky N. J., Scott C. T., Gill B. C., Li C., Podkovyrov V., Maslov A., Konhauser K. O., Lalonde S. V., Love G. D., Poulton S. W. and Lyons T. W. (2013) Large-scale fluctuations in Precambrian atmospheric and oceanic oxygen levels from the record of U in shales. *Earth Planet. Sci. Lett.*, 284–293.

Planavsky N. J., Rouxel O. J., Bekker A., Hofmann A., Little C. T. S. and Lyons T. W. (2012) Iron isotope composition of some Archean and Proterozoic iron formations. *Geochim. Cosmochem. Acta* **80**, 158–169.

Polyakov V. B., Clayton R. N., Horita J. and Mineev S. D. (2007) Equilibrium iron isotope fractionation factors of minerals: reevaluation from the data of nuclear inelastic resonant X-ray scattering and Mössbauer spectroscopy. *Geochim. Cosmochem. Acta* **71**, 3833–3846.

Polyakov V. B. and Soultanov D. M. (2011) New data on equilibrium iron isotope fractionation among sulfides: constraints on mechanisms of sulfide formation in hydrothermal and igneous rocks. *Geochim. Cosmochem. Acta* **75**, 1957–1974.

Poulton S. W. and Canfield D. E. (2005) Development of a sequential extraction procedure for iron: implications for iron partitioning in continentally derived particulates. *Chem. Geol.* **214**, 209–221.

Poulton S. W. and Canfield D. E. (2011) Ferruginous conditions: a dominant feature of the ocean through Earth's history. *Elements* **7**, 107–112.

Poulton S. W. and Raiswell R. (2002) The low-temperature geochemical cycle of iron: from continental fluxes to marine sediment deposition. *Am. J. Sci.* **302**, 774–805.

Radic A., Lacan F. and Murray J. W. (2011) Iron isotopes in the seawater of the equatorial Pacific ocean: new constraints for the oceanic iron cycle. *Earth Planet. Sci. Lett.* **306**, 1–10.

Raiswell R. (2011a) Iceberg-hosted nanoparticulate Fe in the Southern Ocean: mineralogy, origin, dissolution kinetics and source of bioavailable Fe. *Deep-Sea Res. II* **58**, 1364–1375.

Raiswell R. (2011b) Iron transport from the continents to the open Ocean: the Aging-Rejuvenation cycle. *Elements* **7**, 101–106.

Raiswell R. and Canfield D. E. (1998) Sources of iron for pyrite formation in marine sediments. *Am. J. Sci.* **298**, 219–245.

Raiswell R. and Canfield D. E. (2012) The iron biogeochemical cycle past and present. *Geochem. Perspect.* **1**(1), 1–220.

Raiswell R., Newton R., Bottrell S. H., Coburn P. M., Briggs D. E. G., Bond D. P. G. and Poulton S. W. (2008) Turbidite depositional influences on the diagenesis of Beecher's Trilobite Bed and the Hunsrück Slate; sites of soft tissue pyritization. *Am. J. Sci.* **308**(2), 105–129.

Rasmussen B. and Buick R. (1999) Redox state of the Archean atmosphere: evidence from detrital heavy minerals in ca. 3250–2750 Ma sandstones from the Pilbara Craton, Australia. *Geology* **27**(2), 115–118.

Reinhard C. T., Lalonde S. V. and Lyons T. W. (2013) Oxidative sulfide dissolution on the early Earth. *Chem. Geol.* **362**, 44–55.

Reinhard C. T., Planavsky N. J., Gill B. C., Ozaki K., Robbins L. J., Lyons T. W., Fischer W. W., Wang C., Cole D. B. and Konhauser K. O. (2017) Evolution of the global phosphorus cycle. *Nature* **541**, 386–389.

Roden E. E. (2004) Analysis of long-term bacterial vs. chemical Fe (III) oxide reduction kinetics. *Geochim. Cosmochem. Acta* **68** (15), 3205–3216.

Rouxel O. J., Bekker A. and Edwards K. J. (2005) Iron isotope constraints on the Archean and Paleoproterozoic Ocean redox state. *Science* **307**, 1088–1091.

Rouxel O. J., Sholkovitz E. R., Carette M. and Edwards K. J. (2008) Iron isotope fractionation in subterranean estuaries. *Geochim. Cosmochem. Acta* **72**, 3413–3430.

Rustad J. R., Casey W. H., Yin Q.-Z., Bylaska E. J., Felmy A. R., Bogatko S. A., Jackson V. E. and Dixon D. A. (2010) Isotopic fractionation of Mg^{2+}(aq), Ca^{2+}(aq), and Fe^{2+}(aq) with carbonate minerals. *Geochim. Cosmochem. Acta* **74**, 6301–6323.

Sahoo S. K., Planavsky N. J., Jiang G., Kendall B., Owens J. D., Wang X., Shi X., Anbar A. D. and Lyons T. W. (2016) Oceanic oxygenation events in the anoxic Ediacaran ocean. *Geobiology*. http://dx.doi.org/10.1111/gbi.12182.

Sahoo S. K., Planavsky N. J., Kendall B., Wang X., Shi X., Scott C. T., Anbar A. D., Lyons T. W. and Jiang G. (2012) Ocean oxygenation in the wake of the Marinoan glaciation. *Nature* **489**, 546–549.

Saito M. A., Noble A. E., Tagliabue A., Goepfert T. J., Lamborg C. H. and Jenkins W. J. (2013) Slow-spreading submarine ridges in the South Atlantic as a significant oceanic iron source. *Nat. Geosci.* **6**, 775–779.

Schauble E. A., Rossman G. R. and Taylor H. P. (2001) Theoretical estimates of equilibrium Fe-isotope fractionations from vibrational spectroscopy. *Geochim. Cosmochem. Acta* **65** (15), 2487–2497.

Scholz F., McManus J., Mix A. C., Hensen C. and Schneider R. R. (2014a) The impact of ocean deoxygenation on iron release from continental margin sediments. *Nat. Geosci.* **7**, 433–437.

Scholz F., Severmann S., McManus J. and Hensen C. (2014b) Beyond the Black Sea paradigm: the sedimentary fingerprint of an open-marine iron shuttle. *Geochim. Cosmochem. Acta* **127**, 368–380.

Schwertmann U. (1988) Occurrence and formation of iron oxides in various pedoenvironments. In *Iron in Soils and Clay minerals* (eds. J. W. Stucki, B. A. Goodman and U. Schwertmann). D. Reidel Publishing Company, Boston, pp. 267–396.

Severmann S., Johnson C. M., Beard B. L., German C. R., Edmonds H. M., Chiba H. and Green D. R. H. (2004) The

effect of plume processes on the iron isotope composition of hydrothermally derived Fe in the deep ocean as inferred from the Rainbow vent site, Mid-Atlantic Ridge, 36°14'N. *Earth Planet. Sci. Lett.* **225**, 63–76.

Severmann S., Johnson C. M., Beard B. L. and McManus J. (2006) The effect of early diagenesis on the Fe isotope compositions of porewaters and authigenic minerals in continental margin sediments. *Geochim. Cosmochim. Acta* **70**, 2006–2022.

Severmann S., Lyons T. W., Anbar A. D., McManus J. and Gordon G. (2008) Modern iron isotope perspective on the benthic iron shuttle and the redox evolution of ancient oceans. *Geology* **36**(6), 487–490.

Severmann S., McManus J., Berelson W. M. and Hammond D. E. (2010) The continental shelf iron flux and its isotope composition. *Geochim. Cosmochem. Acta* **74**, 3984–4004.

Sharma M., Polizzotto M. and Anbar A. D. (2001) Iron isotopes in hot springs along the Juan de Fuca Ridge. *Earth Planet. Sci. Lett.* **194**, 39–51.

Sholkovitz E. R., Boyle E. A. and Price N. B. (1978) The removal of dissolved humic acids and iron during estuarine mixing. *Earth Planet. Sci. Lett.* **40**, 30–136.

Skulan J. L., Beard B. L. and Johnson C. M. (2002) Kinetic and equilibrium Fe isotope fractionation between aqueous Fe(III) and hematite. *Geochim. Cosmochem. Acta* **66**(17), 2995–3015.

Sossi P. A., Nebel O. and Foden J. (2016) Iron isotope systematics in planetary reservoirs. *Earth Planet. Sci. Lett.* **452**, 295–308.

Sperling E. A., Carbone C., Johnston D. T., Narbonne G. M. and Macdonald F. A. (2016) Oxygen, time and facies controls on the appearance of the Cryogenian and Ediacaran body and trace fossils in the Mackenzie Mountains, Northwest Territories, Canada. *Geol. Soc. Am. Bull.* **128**(3–4), 558–575.

Sperling E. A., Halverson G. P., Knoll A. H., Macdonald F. A. and Johnston D. T. (2013) A basin redox transect at the dawn of animal life. *Earth Planet. Sci. Lett.*, 143–155.

Sperling E. A., Wolock C. J., Morgan A. S., Gill B. C., Kunzmann M., Halverson G. P., Macdonald F. A., Knoll A. H. and Johnston D. T. (2015) Statistical analysis of iron geochemical data suggests limited Late Proterozoic oxygenation. *Nature* **523**, 451–454.

Staubwasser M., von Blankenburg F. and Schoenberg R. (2006) Iron isotopes in the early marine diagenetic iron cycle. *Geology* **34**(8), 629–632.

Stucki J. W., Komadel P. and Wilkinson H. T. (1987) Microbial reduction of structural iron(III) in smectites. *J. Soil Sci. Soc. Am.* **51**, 1663–1665.

Tagliabue A., Bopp L. and Aumont O. (2009) Evaluating the importance of atmospheric and sedimentary iron sources to Southern Ocean biogeochemistry. *Geophys. Res. Lett.* **36**(13), L13601.

Tahata M., Sawaki Y., Yoshiya K., Nishizawa M., Komiya T., Hirata T., Yoshida N., Maruyama S. and Windley B. F. (2015) The marine environments encompassing the Neoproterozoic glaciations: evidence from C, Sr and Fe isotope ratios in the Hecla Hoek Supergroup in Svalbard. *Precambrian Res.* **263**, 19–42.

Tamura Y., Ito K. and Katsura T. (1983) Transformation of γ-FeO(OH) to Fe_3O_4 by adsorption of iron(II) ion on γ-FeO(OH). *J. Chem. Soc. Dalton Trans.* **1983**, 189–194.

Tangalos G. E., Beard B. L., Johnson C. M., Alpers C. N., Shelobolina E. S., Xu H., Konishi H. and Roden E. E. (2010) Microbial production of isotopically light iron(II) in a modern chemically precipitated sediment and implications for isotopic variations in ancient rocks. *Geobiology* **8**, 197–208.

Teutsch N., von Gunten U., Porcelli D., Cirpka O. A. and Halliday A. N. (2005) Adsorption as a cause for iron isotope fractionation in reduced groundwater. *Geochim. Cosmochem. Acta* **69**(17), 4175–4185.

Thamdrup B. (2000) Bacterial manganese and iron reduction in aquatic sediments. In *Advances in Microbial Ecology* (ed. B. Schink). Kluwer Academic/Plenum Publishers.

Toner B. M., Fakra S. C., Manganini S. J., Santelli C. M., Marcus M. A., Moffett J. W., Rouxel O. J., German C. R. and Edwards k. J. (2009) Preservation of iron(II) by carbon-rich matrices in a hydrothermal plume. *Nat. Geosci.* **2**, 197–201.

Vernikovsky V. A. and Vernikovskaya A. E. (2006) Tectonics and Evolution of granotoid mamagmatism in the Yenisei Ridge. *Russian Geol. Geophys.* **47**(1), 32–52.

Vorhies J. S. and Gaines R. R. (2009) Microbial dissolution of clay minerals as a source of iron and silica in marine sediments. *Nat. Geosci.* **2**, 221–225.

Wallmann K., Hennies K., König I., Petersen W. and Knauth H. D. (1993) New procedure for determining reactive Fe(III) and Fe(II) minerals in sediments. *Limnol. Oceanogr.* **38**(8), 1803–1812.

Welch S. A., Beard B. L., Johnson C. M. and Braterman P. S. (2003) Kinetic and equilibrium Fe isotope fractionation between aqueous Fe(II) and Fe(III). *Geochim. Cosmochem. Acta* **67**(22), 4231–4250.

Wiesli R. A., Beard B. L. and Johnson C. M. (2004) Experimental determination of Fe isotope fractionation between aqueous Fe (II), siderite, and "green rust" in abiotic systems. *Chem. Geol.* **211**, 343–362.

Wijsman J. W. M., Middleburg J. J. and Heip C. H. R. (2001) Reactive iron in Black Sea sediments: implications for iron cycling. *Marine Geol.* **172**, 167–180.

Wu L., Beard B. L., Roden E. E. and Johnson C. M. (2009) Influence of pH and Si on Fe isotope fractionation during dissimilatory microbial reduction of hematite. *Geochim. Cosmochem. Acta* **73**, 5584–5599.

Wu L., Beard B. L., Roden E. E. and Johnson C. M. (2011) Stable iron isotope fractionation between aqueous Fe(II) and hydrous ferric oxide. *Environ. Sci. Technol.* **45**, 1847–1852.

Wu L., Beard B. L., Roden E. E., Kennedy C. B. and Johnson C. M. (2010) Stable Fe isotope fractionations produced by aqueous Fe(II)-hematite surface interactions. *Geochim. Cosmochem. Acta* **74**, 4249–4265.

Wu L., Druschel G., Findlay A., Beard B. L. and Johnson C. M. (2012) Experimental determination of iron isotope fractionations among Fe^{2+}_{aq}-FeS_{aq}-Mackinawite at low temperatures: implications for the rock record. *Geochim. Cosmochem. Acta* **89**, 46–61.

Yamaguchi K. E. and Ohmoto H. (2006) Comment on "Iron isotope constraints on the Archean and Paleoproterozoic ocean redox state. *Science* **311**, 177.

Zhang F., Zhu X., Yan B., Kendall B., Peng X., Li J., Algeo T. J. and Romaniello S. J. (2015) Oxygenation of a Cryogenian ocean (Nanhua Basin, South China) revealed by pyrite Fe isotope compositions. *Earth Planet. Sci. Lett.* **429**, 11–19.

Zhu X.-K., O'Nions R. K., Guo Y. and Reynolds B. C. (2000) Secular variation of iron isotopes in North Atlantic deep water. *Science* **287**, 2000–2002.

Associate editor: Nicolas Dauphas